THE UNIVERSITY OF MICHIGAN

INDUSTRY PROGRAM OF THE COLLEGE OF ENGINEERING

ASSOCIATED PRODUCTION OF STRANGE PARTICLES BY NEGATIVE PI MESONS

John L. Brown

A dissertation submitted in partial fulfillment
of the requirements for the degree of
Doctor of Philosophy in the
University of Michigan
1958

March, 1958

IP - 271

ensm

UMR 8617

Doctoral Committee:

Professor Donald A. Glaser, Chairman
Professor Robert C. F. Bartels
Professor Wayne E. Hazen
Associate Professor Paul V. C. Hough
Professor George E. Uhlenbeck

ACKNOWLEDGMENTS

Since this experiment was so largely the result of cooperative group effort, the author is indebted to a large number of people. Thanks are due to the members of the Brookhaven National Laboratory staff for hospitality shown during the author's six month stay there, for assistance from members of the Cosmotron Department (especially Drs. G. B. Collins and W. H Moore) and members of the Physics Department (especially Drs. S. Goudsmit and R. P. Shutt). The aid of Profs. M. L. Perl and D. I. Meyer in setting up and performing the experiment is appreciated.

In addition to the direct assistance mentioned above, the efforts of a number of others were equally needed and appreciated. Gratitude is due to Dr. D. C. Rahm who during his graduate years at Michigan taught the author much of the craft of experimental physics. The patience of the Physics Shop under the direction of Mr. H. Roemer in constructing much of the apparatus and making the endless revisions necessary is acknowledged.

Finally, there is a debt to Prof. D. A. Glaser without whose enthusiasm and guidance the apparatus would never have been built, the experiment set up, or the data analyzed, and who disclosed to the author whatever enjoyment there is in high energy physics.

TABLE OF CONTENTS

TABLE OF CONTENTS CONT'D

LIST OF TABLES

LIST OF FIGURES

LIST OF FIGURES CONT'D

* For derivation of the above graphs see Appendix A.

** For data on individual events see Appendix B.

I. INTRODUCTION

1.1 Historical Background

Within the past ten years quite a few particles have been discovered which are fundamental in the sense that they are resonably stable, and in the sense that their internal structure has not been revealed. Study of the properties of elementary particles may lead one eventually to an underlying theory explaining the existence and properties of these particles.

1947 saw the addition to the list of fundamental particles of the π meson, which is connected with the problem of nuclear forces. 1947 also was the year of the discovery by Rochester and Butler (1) of two examples of what were later termed "V-particles". In a magnetic cloud chamber they observed the decay of a neutral particle into two charged particles, neither of which was a proton. The mass of the neutral particle was calculated to lie in the range 770-1600 m_e (electron masses). These properties could not be ascribed to any particle known at that time. They also found a case of a positively charged particle with a mass in the range 980-1800 m_e, decaying into what was probably a charged π meson and an unknown neutral particle. These properties were also not characteristic of any particle then known. For three years these were the only published examples of what later proved to be a complex class of particles, known as "strange particles". Then in 1950 and 1951 confirmation of the existence of these new particles came from a number of sources. Since at this time strange particles were seen only in cosmic rays, the rate of data collection was slow. On the other hand, the π meson (also discovered

in 1947) was produced by particle accelerators as early as 1948; consequently information concerning the properties of π mesons accumulated much more rapidly. In 1953, however, the first artificial strange particles were produced at the Cosmotron at Brookhaven National Laboratory, and this ushered in a period of more rapid data collection. With counters, cloud chambers, and photographic emulsions as the most common experimental tools, the properties shown in Table 1 were ascertained.

In a field as fast-moving as high-energy physics is today, it is impossible to write down such a table and hope to have it either correct or complete. No attempt has been made in compiling this table to combine rigorously the results of all experiments; for this reason no errors are quoted. Data for this table is taken largely from Reference 2 (and hence represents information as of April, 1956), although more recent data (3)(4) has been added in those cases where the information is relevant to the experiment described in this thesis.

1.2 Some Present-Day Theoretical Ideas Concerning Strange Particles

From cosmic ray data it is known that in high-energy penetrating showers the frequency of occurrence of all V particles is about 1 - 10% of that of π mesons. If the production of π mesons is postulated to arise from a "strong" interaction (i.e., one with a large coupling constant, taken for purposes of further discussion as 1 in some units) and if strange particles decay with the same strength interaction which produced them, one might expect lifetimes of the order of 10^{-21} sec. Experimentally, however, as seen from Table 1, most strange particles

TABLE 1. SOME PROPERTIES OF STRANGE PARTICLES

Name	Mass (Mev.)	Lifetime (secs.)	Decay Modes
K^+	494	1.2×10^{-8}	$\theta^+ \rightarrow \pi^+ + \pi^\circ$ $\tau^+ \rightarrow \pi^+ + \pi^+ + \pi^-$ $K^+_{\mu 2} \rightarrow \mu^+ + \nu$ $K^+_{\mu 3} \rightarrow \mu^+ + \pi^\circ + \nu$ $K^+_{e3} \rightarrow e^+ + \pi^\circ + \nu$ $\tau^{+\prime} \rightarrow \pi^+ + \pi^\circ + \pi^\circ$
K^-	494	1.2×10^{-8}	presumably same kinds as K^+
θ°	494	--	$\theta^\circ_1 \rightarrow \pi^+ + \pi^-$ lifetime
$\overline{\theta^\circ}$	494	--	$\rightarrow \pi^\circ + \pi^\circ$ 1.7×10^{-10} sec. - - - - - - - - - - - - - $\theta^\circ_2 \rightarrow$ three body decays lifetime $\sim 10^{-7}$ sec.
Λ°	1115	$\sim 3 \times 10^{-10}$	$\Lambda^\circ \rightarrow p + \pi^-$ $\rightarrow n + \pi^\circ$ (?)
Σ^+	1189	$\sim 1 \times 10^{-10}$	$\Sigma^+ \rightarrow p + \pi^\circ$ $\rightarrow n + \pi^+$
Σ°	1190	$\ll 10^{-10}$	$\Sigma^\circ \rightarrow \Lambda^\circ + \gamma$
Σ^-	1197	1.8×10^{-10}	$\Sigma^- \rightarrow n + \pi^-$
Ξ^-	1321	$\sim 10^{-10}$	$\rightarrow \Lambda^\circ + \pi^-$

decay with lifetimes of the order of 10^{-8} to 10^{-10} seconds.

Several explanations of this discrepancy have been put forth. The "strangeness" hypothesis is the one which seems to be experimentally verified. According to this hypothesis one assigns a new quantum number (usually called "strangeness") to all elementary particles, and postulates certain selection rules concerning this quantum number. Values of this quantum number S, assigned ad hoc to fit the experimental results, are quoted in Table 2. (There is no unanimity in the literature concerning the choice of the new quantum number, but we shall follow the convention of Reference 2).

Also listed are values of T and T_z, the total isotopic spin and its z component, respectively. These have been assigned assuming that the three Σ particles, for example, which have nearly the same mass, are mass multiplets. The small differences in mass might then be caused by electromagnetic interactions (whose strength is about 1/137 in the same units as used in discussing strong interactions) which depend upon T_z. If one accepts these assignments, the charge of a particle (in terms of the magnitude of the electronic charge) is given by:

$$Q = T_z + S/2 + M/2$$

where M is the so-called baryon number (+1 for nucleons and hyperons, -1 for anti-nucleons and anti-hyperons, and 0 for all other particles).

One now postulates selection rules concerning the strangeness S. One asserts that for strong interactions (e.g., strange particle production), $\Delta S = 0$. For weak interactions (e.g., strange particle decay,), which are characterized by strengths $\sim 10^{-13}$, we have $\Delta S = \pm 1$.

Thus strange particles ($S \neq 0$) cannot decay into pions, nucleons, etc., ($S = 0$) via strong interactions and hence will have relatively long lifetimes.

Some fast (strong interaction) reactions permitted by the selection rule $\Delta S = 0$ are:

$$\pi^- + p \rightarrow \Lambda^\circ + \Theta^+$$
$$\pi^- + p \rightarrow \Sigma^- + K^+ \qquad \text{associated production}$$
$$\pi^- + p \rightarrow \Sigma^\circ + \Theta^\circ$$
$$K^- + p \rightarrow \Lambda^\circ + \pi^\circ$$
$$K^- + p \rightarrow \Sigma^- + \pi^+$$
$$K^- + p \rightarrow \Sigma^\circ + \pi^\circ \qquad K^- \text{ absorption}$$
$$K^- + p \rightarrow \Sigma^+ + \pi^-$$

whereas:

$$\pi^- + p \rightarrow \Sigma^+ + K^-$$
$$\pi^- + p \rightarrow \Lambda^\circ + \pi^\circ$$

are forbidden as fast reactions. We note that:

$$\Sigma^\circ \rightarrow \Lambda^\circ + \gamma$$

will be fast, since $\Delta S = 0$, so that the Σ° will have a very short lifetime.

$$\Sigma^+ \rightarrow \Lambda^\circ + \pi^+$$
$$\Sigma^- \rightarrow \Lambda^\circ + \pi^-$$

would also be fast except for the fact that they are endothermic, i.e. there is not enough energy available.

TABLE 2 STRANGENESS AND ISOTOPIC SPIN ASSIGNMENTS

Particle	Strangeness (S)	Total Isotopic Spin (T)	z-Component of Isotopic Spin (T_z)
θ°	+1	1/2	-1/2
$\overline{\theta}^\circ$	-1	1/2	+1/2
K^+	+1	1/2	1/2
K^-	-1	1/2	-1/2
Λ°	-1	0	0
Σ^+	-1	1	+1
Σ°	-1	1	0
Σ^-	-1	1	-1
Ξ^-	-2	1/2	-1/2
N, e, μ, π ν, γ, etc.	0		

To date no reaction has been found which contradicts the predictions above; all the strong interactions have $\Delta S = 0$, while the weak decay interactions have $\Delta S = \pm 1$. No weak production interactions have been found since presumably their cross sections are undetectably with present experimental techniques.

A second difficulty arising from the experimental facts concerns the K^+ particles. Experimentally the K^+ particles have the same mass and lifetime (within experimental errors), the same strangeness, and the same isotopic spin. They are distinguished by their decay modes, but the parent particle is presumably the same in all cases. Two particular decay modes present a problem, however:

$$\theta^+ \rightarrow \pi^+ + \pi^\circ$$

$$\tau^+ \rightarrow \pi^+ + \pi^+ + \pi^-$$

Because of the difference in decay schemes, they cannot <u>both</u> have the same parity if they both have intrinsic spin 0. Further, because of the experimentally known energy and angular distributions of the τ^+, they probably cannot both have the same spin and parity except for unreasonably high values of intrinsic spin ($j \geq 4$)(5), and hence apparently <u>cannot</u> be the same particle exhibiting different decay modes. Then the question arises -- why do we have two particles alike in every respect except for spin and parity?

Two explanations have been offered for this difficulty. One of them (the parity doublet scheme) assumes the θ^+ and the τ^+ have the same spin but opposite parity. One then defines an operator C_p (the parity conjugation operator) which interchanges the θ^+ and τ^+ but leaves nucleons and pions unchanged. One assumes that C_p is an invariant for strong interactions but not for weak interactions. A consequence of this hypothesis is that the θ^+ and τ^+ could have the same mass, lifetime, excitation function, etc., within experimental error. A second consequence is that <u>all</u> particles of odd strangeness would exist in two

states of opposite parity. These two states of opposite parity might manifest themselves in the weak decay interactions.

A second explanation of the "$\theta - \tau$" puzzle is to assume that parity is not conserved in the weak interactions, although it is conserved in strong and electromagnetic interactions. This hypothesis has recently been shown to be true for some weak interactions. Both the parity doublet and parity non-conservation hypotheses might have observable consequences (under favorable conditions) in the experiment described in this thesis.

1.3 Purpose of the Experiment Described in This Thesis

Shutt and collaborators in 1953 (6) and Walker and Shephard (7) investigated the reactions:

$$\pi^- + p \rightarrow \Lambda^\circ + \theta^\circ$$
$$\pi^- + p \rightarrow \Sigma^\circ + \theta^\circ$$
$$\pi^- + p \rightarrow \Sigma^- + K^+$$

in a hydrogen-filled diffusion cloud chamber with and without a magnetic field at pion kinetic energies of 1.0 and 1.4 Bev. They found some twelve cases of strange particle production consistent with the above reactions, which tended to support the hypothesis of associated production predicted by strangeness theory. The cross section for strange particle production was about 0.9 mb for all reactions combined. The angular distribution of production of the $\Lambda\theta$ reaction in the π^--p center of mass system was anisotropic, the Λ° tending to come off in the backward direction. By using the lifetimes for charged short-lived decay modes (obtained from cosmic ray experiments) they concluded that

it was likely that the Λ° and θ° have other decay modes, either neutral:

$$\Lambda^\circ \rightarrow n + \pi^\circ$$

$$\theta^\circ \rightarrow \pi^\circ + \pi^\circ$$

or long-lived (or both). They also found certain angular correlations in the Λ° decay which tended to indicate an intrinsic spin greater than 1/2 for the Λ°.

The experiment described in part in this thesis is an extension of the work done by Shutt and by Walker. We wished to find:

1) the production cross section (total and differential) for

$$\pi^- + p \rightarrow \Lambda^\circ + \theta^\circ$$

$$\pi^- + p \rightarrow \Sigma^\circ + \theta^\circ$$

$$\pi^- + p \rightarrow \Sigma^- + K^+ ;$$

2) the lifetime of the Λ°, θ°, and Σ^-;

3) information concerning the intrinsic spin of the Λ°, θ°, Σ^-;

4) evidence, if any for the existence of parity doublets or parity non-conservation in strange particle decay;

5) the branching ratio of charged to neutral or long-lived decay modes of the Λ° and θ° (not covered in this thesis);

6) π^- - n and π^- - p reactions occurring in carbon (not covered in this thesis).

In order to make it feasible to collect a significant amount of data on strange particle production, a different type of detector than the diffusion cloud chamber would be useful, since the density of hydrogen in such a device is only 0.002 gm/cm^3. This results in a low rate

of production of strange particles and also in low stopping power for the decay secondaries. A propane bubble chamber, on the other hand, has a hydrogen density of 0.08 gm/cm^3 and a total density of 0.44 gm/cm^3 which means that both the production rate and stopping power will be high. Using this device it was felt that a reasonable number of associated production events would be obtained, so that some of the questions mentioned above could be answered experimentally.

II. EXPERIMENTAL APPARATUS AND DESIGN

2.1 The Bubble Chamber

The basic detecting instrument in this experiment was the bubble chamber, an early model of which is described in Reference 8. The chamber used in this experiment was rectangular in shape, with inside dimensions 12" x 5" x 5". The chamber was oriented so that the incident beam traversed the long dimension of the chamber. A schematic drawing of the chamber is shown in Fig. 1. Several features of the chamber, which represent a departure from earlier design, are described below.

In the interests of being able to accurately reconstruct an event in real space from measurements made on the stereoscopic negatives, sets of fiducial marks were deposited on the inner surfaces of the front and back windows. These fiducial marks were placed in a rectangular pattern with a spacing of 1.000 ± 0.001 cm. In order to insure uniformity of the pictures, the camera and chamber were mounted on a rigid steel I-beam frame. 70 mm film was used, in preference to smaller, more convenient sizes, in order to increase measurement accuracy. In order to insure a constant image distance, the film was held in place in the camera by means of vacuum backing. Finally, in order to simplify the reconstruction of events, the positions of the chamber and camera were adjusted with the aid of a transit.

The expansion system differed somewhat from earlier versions because of the larger chamber volume. Compressed air was applied behind a rubber diaphragm on the bottom of the chamber, the top of the dia-

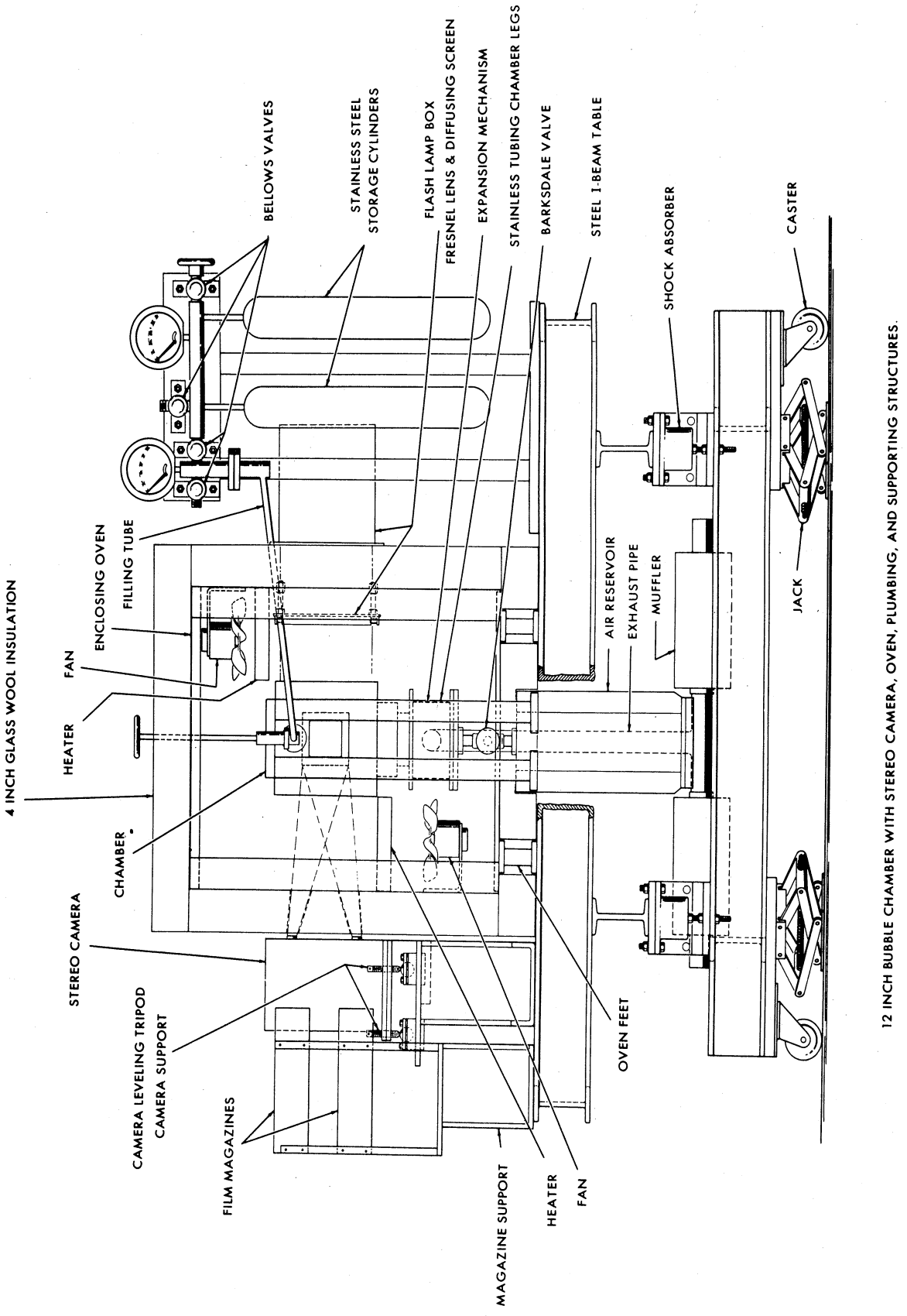

Figure 1a. Overall Schematic Drawing of Bubble Chamber Assembly

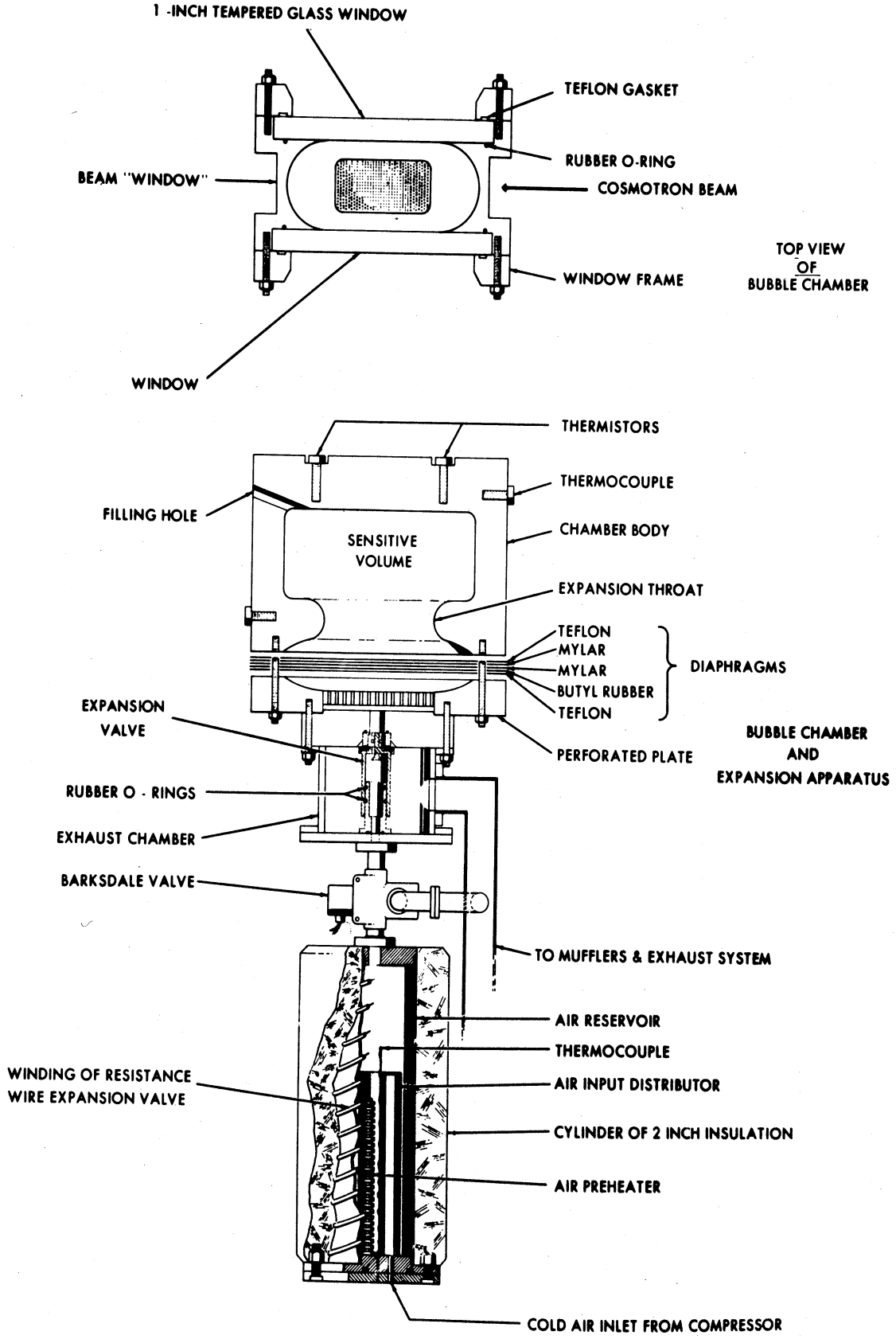

Figure 1b. Detail Schematic Drawing of Chamber Proper

phragm being in contact with the propane. The chamber was expanded by applying an electronic pulse to a commercial 3-way solenoid valve which actuated a home-made valve having a large (1-5/8") port diameter, thus releasing the compressed air into an exhaust system. This system was overly complex and wasteful of compressed air, but after suitable modifications worked reliably and expanded the chamber in roughly 5 milliseconds.

A propane chamber of this size is an extremely hazardous device because of the possibility of a physical explosion due to failure of some part (e.g., a window), followed by ignition of the propane. For this reason it was necessary to install safety devices to prevent overheating the chamber which would cause the pressure to rise to dangerous values due to the thermal expansion of the propane. A commercial combustible vapor detector was also used, which continuously sampled the air around the chamber; if the propane concentration rose to more than one-tenth the lower explosive limit, the detector actuated an alarm, turned off the chamber heating, and released the compressed air.

2.2 Experimental Set-up at the Cosmotron

The data for this experiment was taken at the proton synchrotron (Cosmotron) at Brookhaven National Laboratory. The necessary π^- beam was obtained by allowing the internal circulating proton beam to strike a graphite target located in the south field-free straight section. The particles produced in the target then entered the field of the Cosmotron, where all negative particles were bent out of the machine. Collimators were set up in the Cosmotron shielding to pass pions whose momentum was 1.231 Bev/c. After emerging from the shielding, the beam passed through an 18" x 36" steering magnet, deflecting the beam into

the bubble chamber which was located behind further shielding. A diagram of the experimental arrangement is shown in Fig. 2.

The trajectory through the steering magnet was obtained by the hot wire method, while the trajectory through the Cosmotron field was very kindly calculated for us by R. M. Sternheimer of the Cosmotron Department. The momentum resolution of the overall arrangement was very poor and was improved in succeeding experiments done with other beams. By means described in Chapter III, we found that half of the beam fell within ± 2% of the mean value. It is estimated that perhaps 8% of the beam particles entering the chamber were μ mesons.

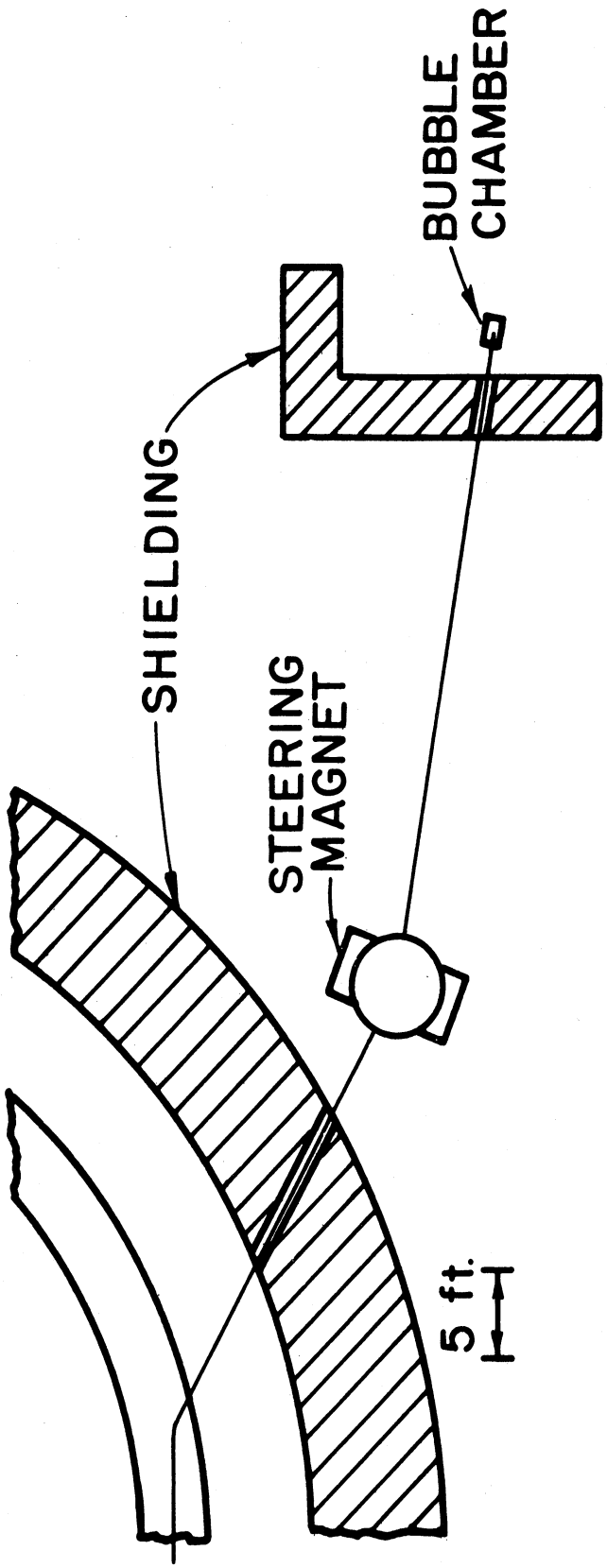

Figure 2. Plan View of Experimental Set-Up.

III. REDUCTION OF DATA; ERROR AND BIAS ANALYSIS

3.1 Scanning and Measurement of Pictures

31,000 pictures were taken in the π^- beam described in Chapter II, with an average of 14.5 tracks per picture. Scanners were instructed to scan along the pion tracks for the following two categories of events.

1. Pion tracks which appeared to end inside the chamber and which were associated with one or more V's, such that a line from the end of the pion track to the vertex of the V fell inside the V. This insured the possibility of balancing transverse momentum. This last requirement introduced a bias against observing three-body decays of V°'s, since both charged particles could conceivably be on the same side of the line of flight of the neutral strange particle, with transverse momentum being balanced by the neutral decay product. For this same reason we were biased against observing scattered V°'s.

2. Y-shaped events, where the stem of the Y represented the incoming pion. Further, it was required that at least one branch of the Y show a kink, representing a possible Σ^- or K^+ decay. In order to reduce the number of double pion scatterings included by this criterion, we added the following two restrictions, which all real $\Sigma^- - K^+$ events had to satisfy: i. the total included angle between the supposed Σ^- and K^+ had to be less than 90°; ii. one track had to make an angle of less than 30° with respect to the incident pion.

Those events selected by the scanners under the above criteria were then rescanned to see if they could be rejected by inspection for any reason. If not, the stereoscopic pairs of film negatives were

measured on a traveling microscope capable of measuring film coordinates to an accuracy of 0.002 in. on the average. Selected points on each event were measured in this way, the film coordinate measurements being transferred to punched cards and processed on an IBM 650 computer. Results obtained from the computer included coordinates in space of each point measured, lengths of line segments, angles between line segments, angles between lines and planes, and angles between planes.

3.2 Identification of $\pi^- + p \rightarrow \Sigma^- + K^+$ Events

$\Sigma^- - K^+$ events occurring in hydrogen, an example of which is shown in Fig. 3, were identified by the criteria described below.

1. The Σ^-, K^+, and incident π^- tracks had to lie in a plane, within measurement errors.

2. The measured angles θ_{Σ^-} and θ_{K^+} had to lie within the range predicted by kinematics as shown in Fig. 4. The finite width of the acceptance band was due to the uncertainty in the incident π^- momentum. A given measurement, if it satisfied requirement 1 and fell within the band, qualified as a potential $\Sigma^- - K^+$ event. From the values of θ_{Σ^-} and θ_{K^+} one could then determine the incident π^- momentum and the center of mass production angle. This in turn determined the momentum, energy, and velocity of the Σ^- and K^+.

Knowing the Σ^- momentum and the angle θ_{π^-} in the laboratory between the Σ^- and the decay π^- from $\Sigma^- \rightarrow \pi^- + n$ one could determine the center of mass angle of the Σ^- decay. This in turn determined the momentum, energy, and velocity of the decay pion.

Thus by measuring θ_{Σ^-}, θ_{K^+}, and θ_{π^-} one could determine the energy and velocity of the incident π^-, the Σ^-, and K^+ and the decay π^- from $\Sigma^- \rightarrow \pi^- + n$. Knowing the energies of these particles one could

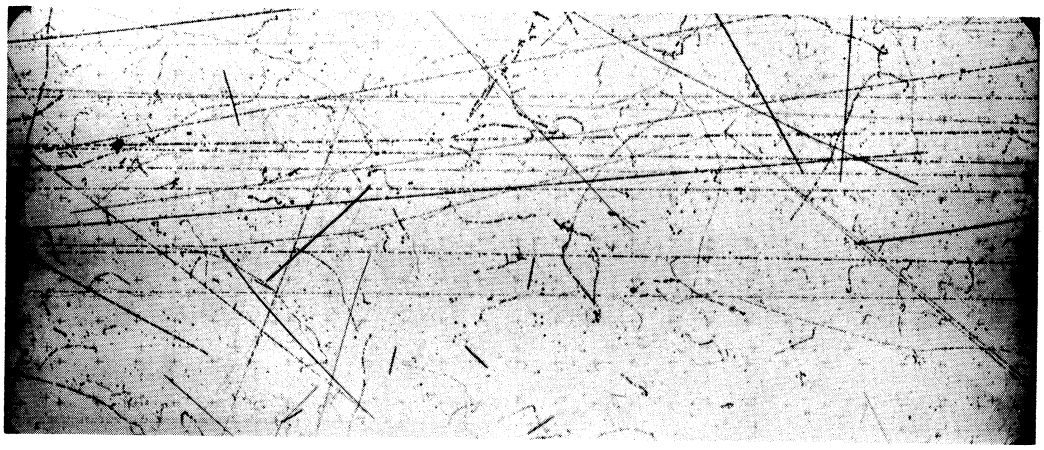

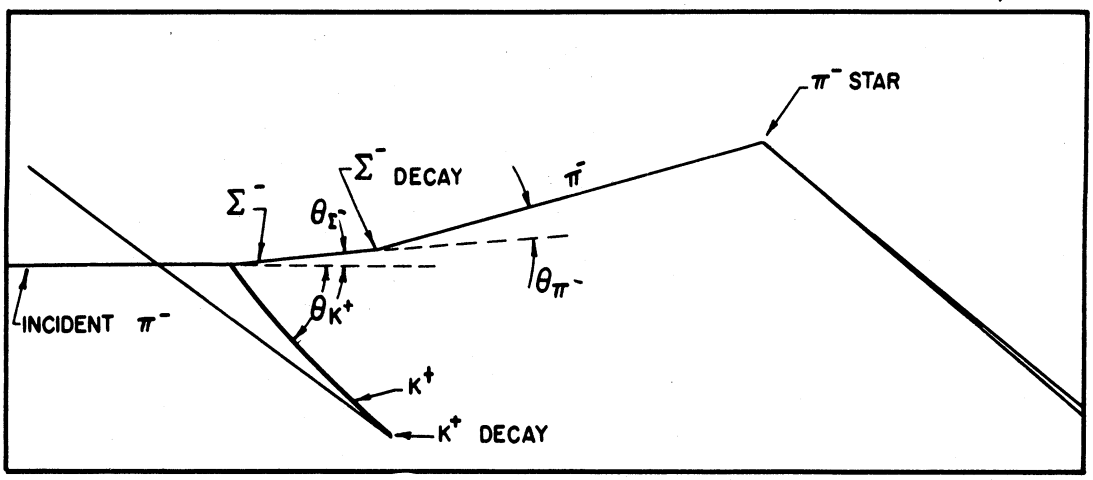

Fig. 3. Sample Σ^- - K^+ Event with Tracing

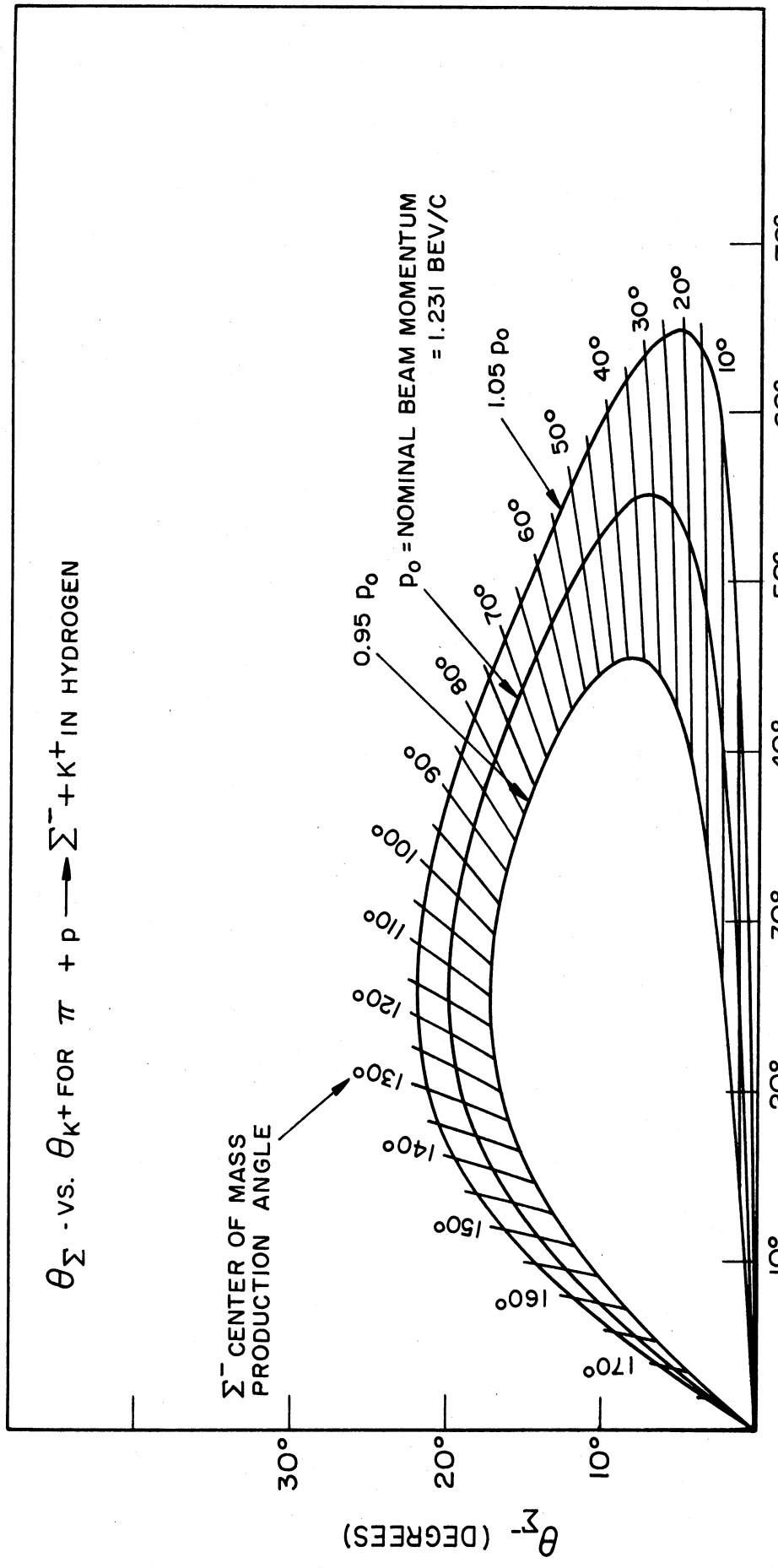

Figure 4. Graph of θ_{Σ^-} vs θ_{K^+} for Reaction $\pi^- + p \rightarrow \Sigma^- + K^+$

predict their range, which had to agree with the measured value. The incident π^- of course never stopped, nor did the Σ^- which either decayed in flight or escaped the chamber. In 8 cases the K^+ stopped and in one case the decay π^- stopped.

The cases in which the K^+ stopped provided an accurate means of checking the incident pion momentum, since the K^+ range was a sensitive function of the incident π^- momentum. Using the 8 cases mentioned we found the π^- beam momentum had a standard deviation of 2.6%.

3. Knowing the velocities of all the particles involved, we could assert something concerning the bubble densities, b, of their tracks. In particular we might predict, say,

$$b(K^+) > b(\Sigma^-) > b(\text{decay } \pi^-) > b(\text{incident } \pi^-)$$

which could be checked using the observed values. All that needed to be assumed in making the above prediction was that the bubble density was a monotonic decreasing function of the velocity. Experiments done on direct bubble counting (9) indicated that the bubble density had the following velocity dependence:

$$b = A/\beta^2 + B$$

where β is the particle velocity (in units of c, the velocity of light), A is a temperature independent constant, and B is a temperature dependent constant. Other experiments have been done (10) in which the distance, x, between bubbles is measured; a Poisson distribution:

$$f(x) = me^{-mx}$$

was found, where m is the average number of bubbles per centimeter. By measuring f(x), one can compute m, which is supposedly the "true" bubble density. m was found to have a velocity dependence consistent with:

$$m = C/\beta^2$$

where C is a temperature dependent constant. Neither of the above formulas (for b and m) was used as such in this experiment because of the difficulty in determining the various constants and because of the generally large statistical errors involved in measuring a given track.

3.3 Identification of $\pi^- + p \rightarrow \Lambda^\circ + \theta^\circ$ Events

An example of a $\Lambda^\circ - \theta^\circ$ event is shown in Fig. 5. It will be noted that we dealt only with those events in which both the neutral V-particles were observed to decay via a two-body charged mode. $\Lambda^\circ - \theta^\circ$ events were identified by means of the following criteria.

1. The production event had to be coplanar, i.e., the lines of flight of the incident π^-, the Λ°, and the $\theta^\bullet$ all had to lie in a plane. Further, the line of flight of the Λ° (or θ°) had to lie in the decay plane formed by the charged decay products of the Λ° (or θ°). This criterion alone usually insured that we were dealing with associated production of some kind.

2. The angles θ_Λ and θ_θ had to fall within a certain kinematically determined acceptance band, as shown in Fig. 6. Again the finite bandwidth is due to the uncertainty in the incident π^- momentum. If a given measurement fell in this band it was a possible hydrogen event, and the corresponding center of mass production angle and beam momentum were read off. These in turn were used to determine the momentum of the Λ° and θ°.

Next, by examining θ_p and θ_{π^-} (or θ_{π^-} and θ_{π^+}) we could determine the momentum and center of mass decay angle of the Λ° (or θ°). These had to agree (within the error) with those determined by examining just the production event.

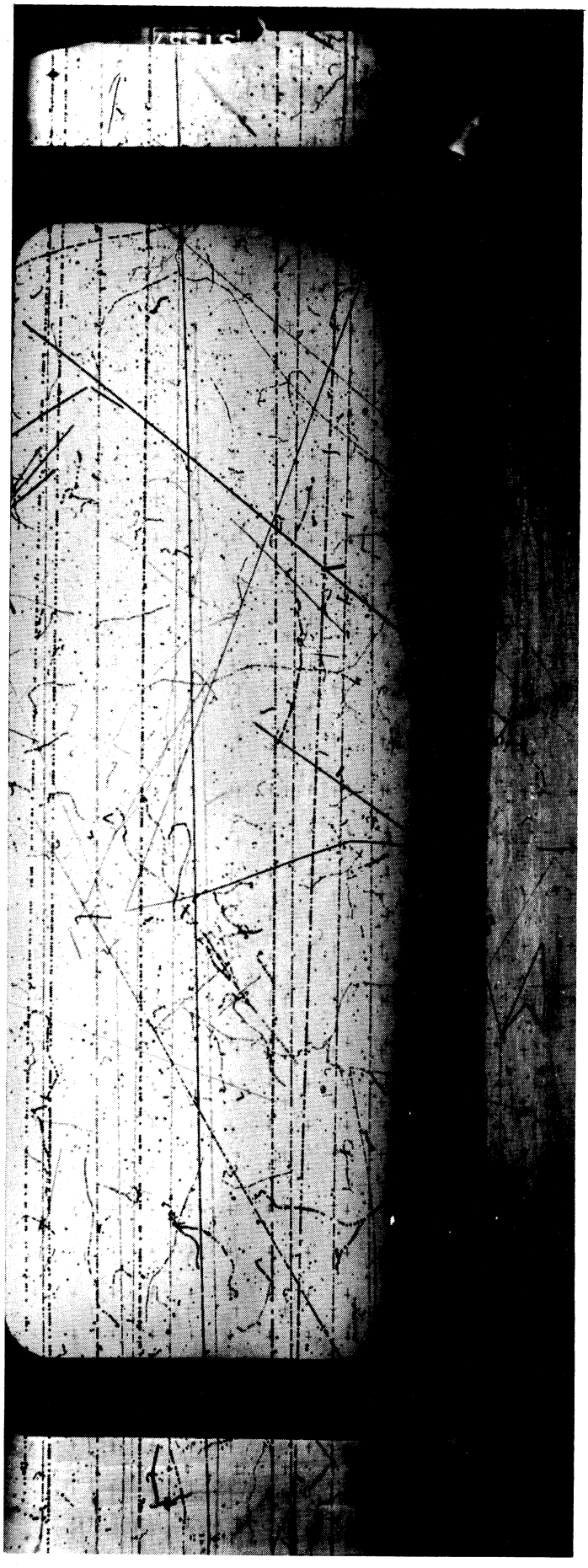

Figure 5a. Sample A° - 0° Event

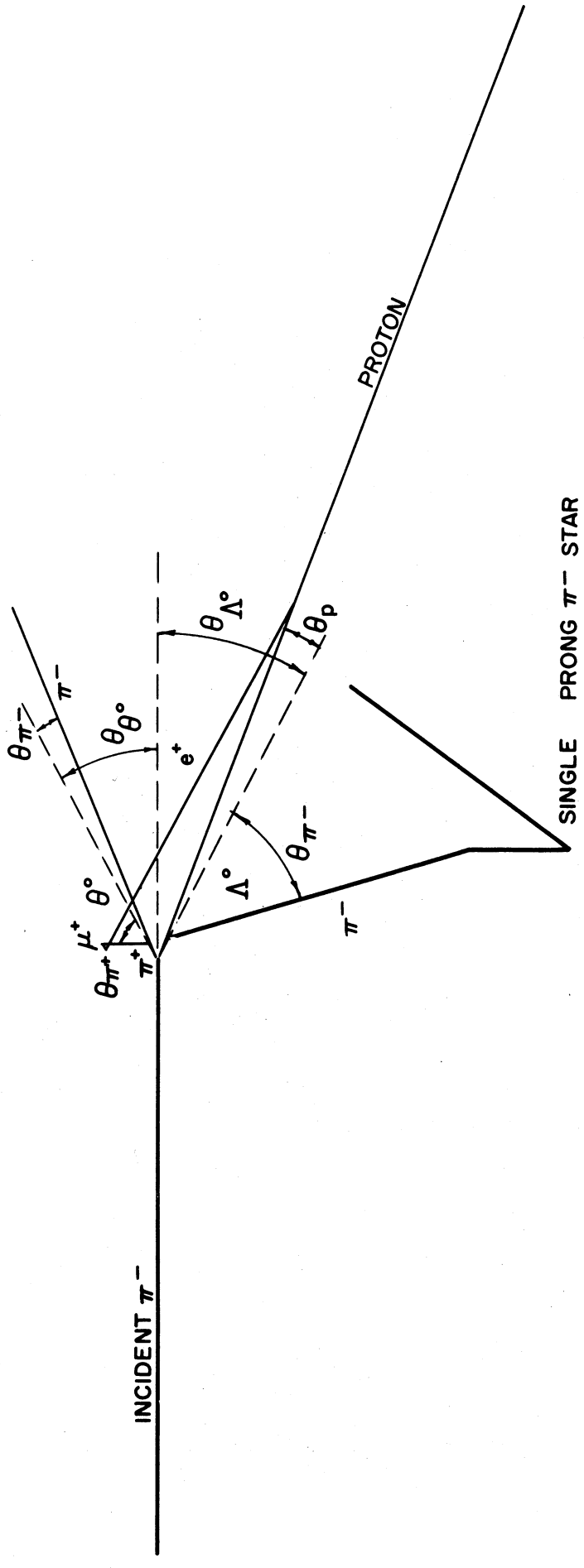

Figure 5b. Tracing of Sample Λ° - θ° Event

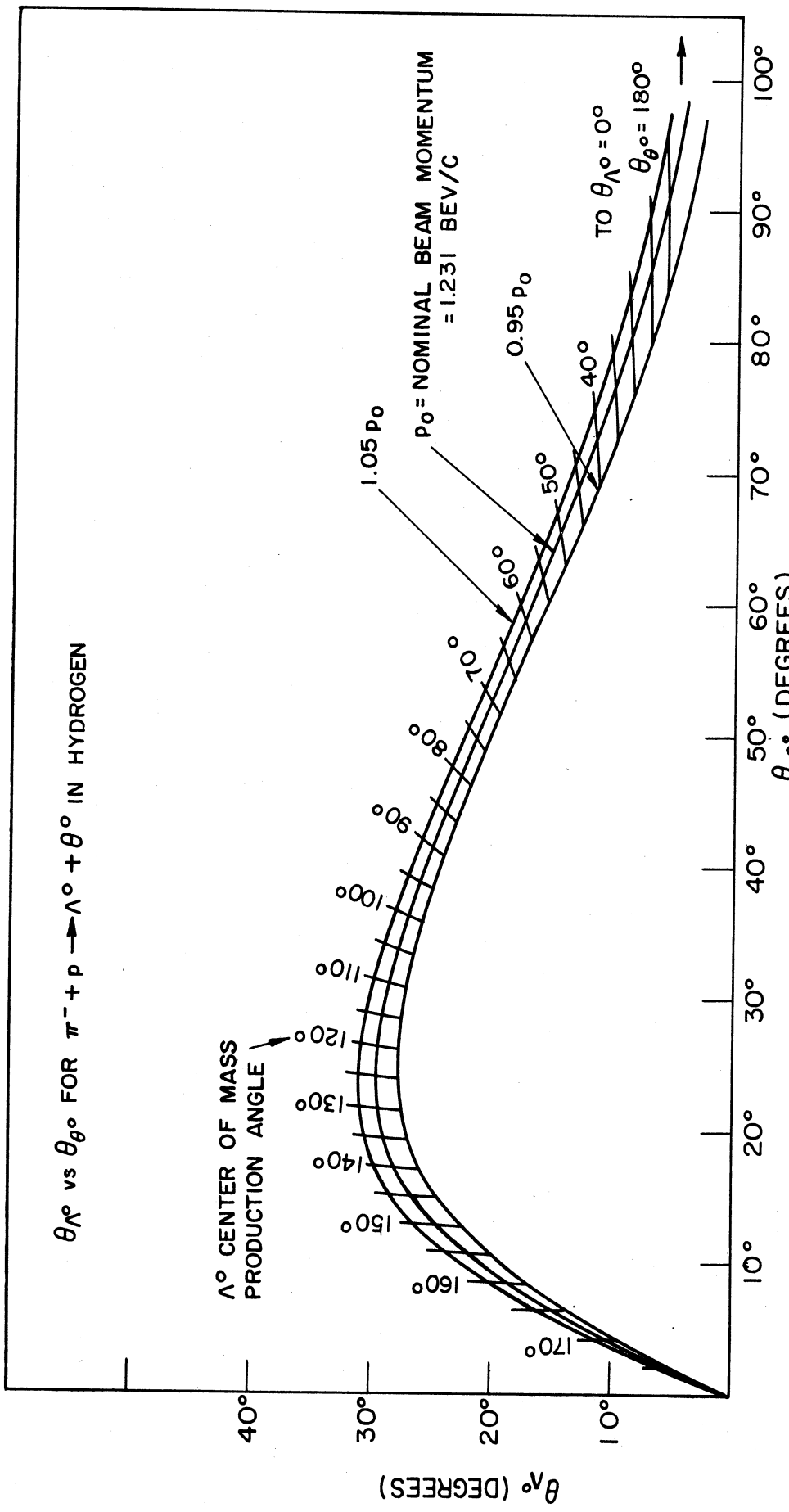

Figure 6 Graph of θ_Λ vs. θ_Θ for Reaction $\pi^- + p \rightarrow \Lambda^\circ + \theta^\circ$

3. Once having found the center of mass decay angles and momenta of the Λ° and θ° we could determine the energies and velocities of the charged decay products ($\Lambda^\circ \rightarrow p + \pi^-$, $\theta^\circ \rightarrow \pi^- + \pi^+$). Then we could compare calculated and observed ranges. In 5 out of 15 events one or more charged particles stopped, so that this was a fairly useful criterion.

4. Knowing the velocities of all the charged particles, we could check the observed and calculated bubble densities in a qualitative way. No events had to be discarded on the basis of this criterion.

3.4 Identification of $\pi^- + p \rightarrow \Sigma^\circ + \theta^\circ$, $\Sigma^\circ \rightarrow \Lambda^\circ + \gamma$

$\Sigma^\circ - \theta^\circ$ events appeared the same to the eye as $\Lambda^\circ - \theta^\circ$ events; a prototype event is sketched in Fig. 7 in order to illustrate certain angles used below. It should be remembered that the Σ° has a very short lifetime ($\sim 10^{-21}$ sec) so that it will decay in $\sim 10^{-11}$ cm. The following criteria were used in the identification of $\Sigma^\circ - \theta^\circ$ events.

1. Presumably the production event ($\pi^- + p \rightarrow \Sigma^\circ + \theta^\circ$) was coplanar if it occurred in hydrogen; what was observed, however, was the $\Lambda^\circ - \theta^\circ$ plane. The Λ° from the $\Sigma^\circ \rightarrow \Lambda^\circ + \gamma$ decay could have fallen anywhere within a cone whose axis was the Σ° line of flight and whose half-angle was 8° or less, depending on the Σ° momentum. Thus the apparent $\pi^- - \Lambda^\circ - \theta^\circ$ production event could have been non-coplanar by as much as 8°. Since this was also true for many cases of $\pi^- + p \rightarrow \Lambda^\circ + \theta^\circ$ in carbon, this criterion was of little value in identification. It was also necessary, however, that the decay planes contain the lines of flight of the neutral V-particles.

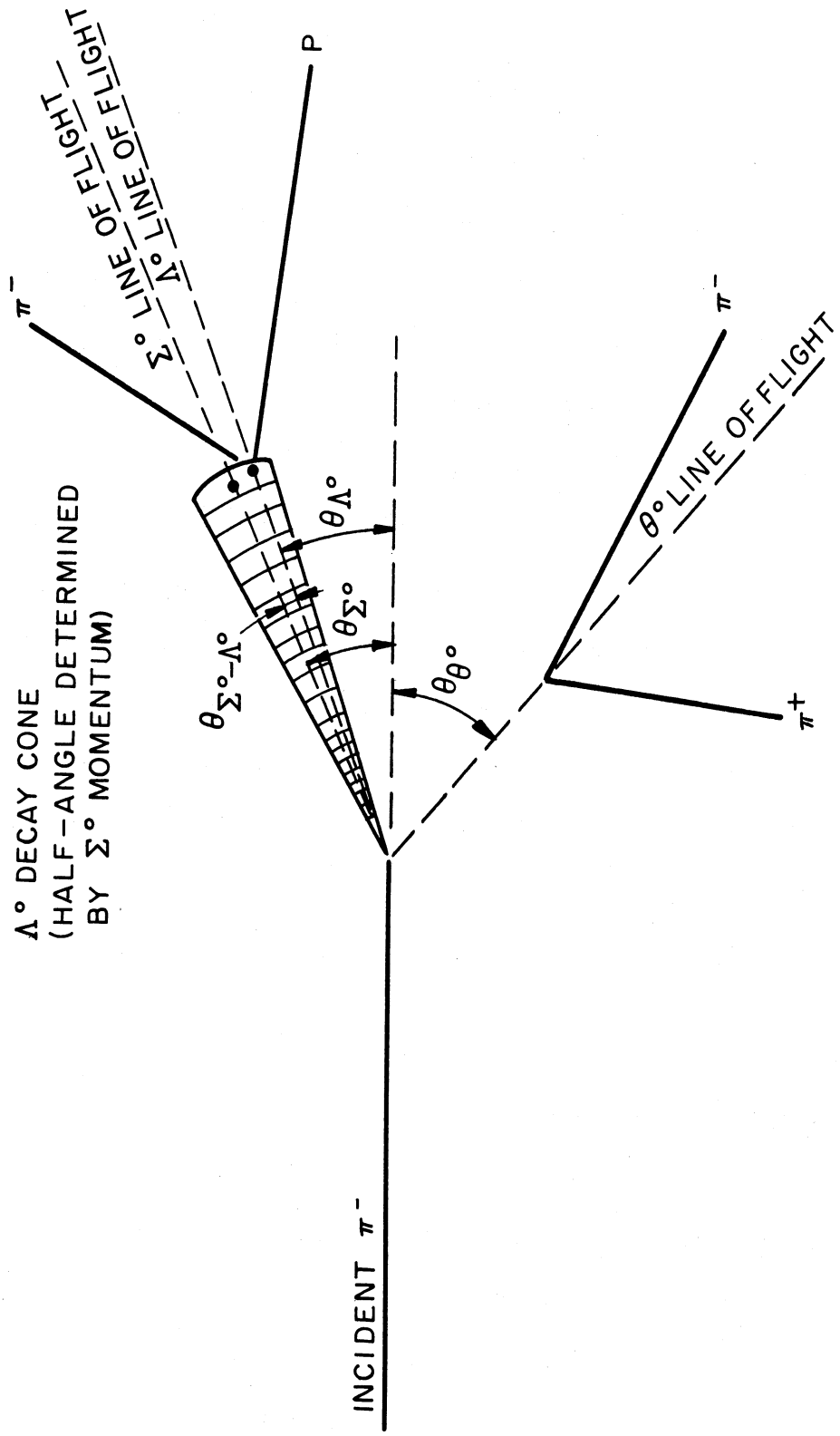

Figure 7 Sketch of Σ° - θ° Event

2. By examining θ_θ, the laboratory production angle of the θ°, one could estimate the center of mass production angle, with some uncertainty due to the spread in beam momentum (see Fig. 8). From this we determined the θ° momentum and compared it with the θ° momentum deduced from the decay event, just as in the case of the Λ° - θ° events.

3. If the above criterion was satisfied, we referred again to Fig. 8 and read off θ_Σ (the laboratory production angle of the Σ°) and also determined the momentum of the Σ°. Knowing these we could kinematically predict the cone within which the Λ° must have fallen, and a range of momenta for the Λ°. In theory we could have used the non-coplanarity of the apparent π^- - Λ° - θ° production event to find the angle between the Λ° and the Σ° lines of flight and thus predict the Λ° momentum exactly, but this angle was always less than 8°, which was not many times greater than the measurement error. This cone of angle for the Λ° and range of possible Λ° momenta was then compared with the observed angle θ_Λ and the momentum determined from the Λ° decay.

4. As in other events, calculated bubble densities and ranges were compared with observed values.

3.5 Discussion of Errors

A common type of experiment consists in making a set of measurements on a large class of known objects as a function of some variable and then deducing some parameter or functional relation concerning the group of measured objects. Thus one might record counter telescope pulses produced by a group of radioactive atoms as a function of some angle and use these to determine a mean life or some angular correlation function. The effect on these conclusions of systematic and random

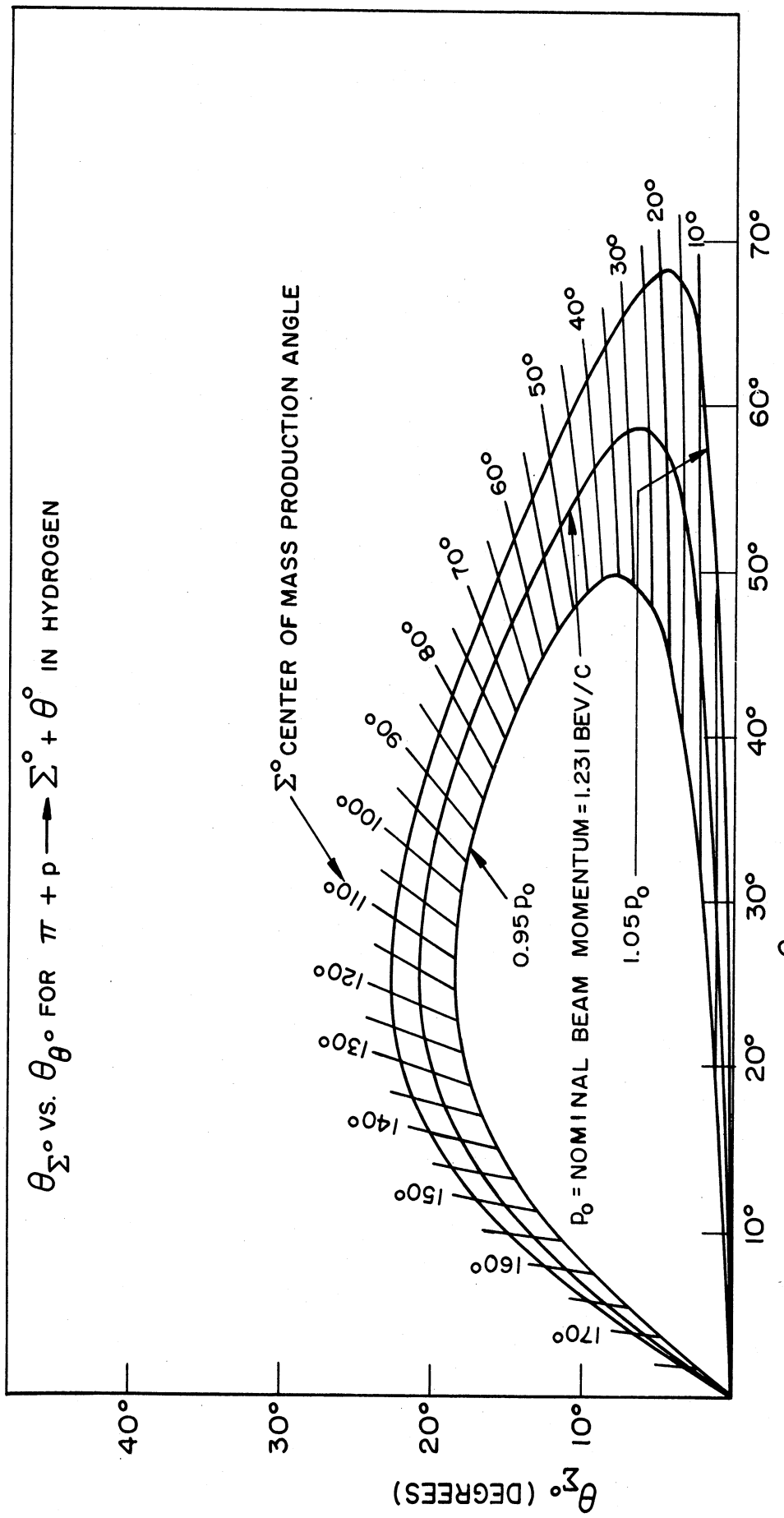

Figure 8. Graph of θ_{Σ° vs. θ_{θ° for Reaction $\pi^- + p \rightarrow \Sigma^\circ + \theta^\circ$

errors in the measurements can then be studied.

This experiment differed rather markedly from the above type. The main difference lay in the fact that the group of objects studied was neither large nor precisely known. In all cases the errors affecting the validity of the results arose from three causes:

1) a very large statistical error due to the small number of events;
2) possible doubts concerning the identity of the objects or events studied; and
3) possible biases which tended to make one observe one class of event more than another.

In this section we will consider the various factors entering into the identification of events. In Section 3.6 we will discuss the possible sources of bias.

The basic direct measurements made in this experiment were the measurements of coordinates on the film negatives. From these measurements, the event was reconstructed in real space. Kinematics then determined the momenta involved, and finally the identity of the event was established. The errors in each of these steps are discussed below.

3.5.1. Basic Measurement Error

Let us consider a double-V event of the type shown in Fig. 9. Points 3 and 6 are the vertices of the V's, point 2 is the end of the incoming pion track, and the other points are chosen by the measurer at his convenience. In addition, the coordinates of the central grid mark are measured. There are a number of possible errors in making these primary measurements:

a) inaccuracies of the microscope scale graduations;

b) non-reproducibility of cross-hair settings;

c) obscuring of the desired point by other tracks;

d) misalignment of film axes with directions of microscope travel; and

e) difficulty in identifying corresponding bubble images due to bubbles being fused, poorly illuminated or out of focus.

3.5.2 Real Space Errors

A. The rectangular coordinates of a point in real (or bubble chamber) space, denoted by X, Y, and Z (to be defined later) can be found by making measurements of the image of that point on each of the stereographic film negatives. The relationship between the film measurements and the real space coordinates can be derived exactly and the various constants entering it evaluated if one knows all the indices of refraction, lens aberrations, image distances, object distances, and so forth. This is impractical, since many of these quantities are not easily measurable. A second approach would be to simply expand X, Y and Z in a power series in terms of coordinates measured on the film, and then determine the expansion coefficients by inserting the film coordinates measured for images of points in real space whose X, Y and Z are known.

The third method, and the one used in practice, combines some of the features of both. One writes down the exact relation between X, Y and Z and film coordinates in terms of various image and object distances, indices of refraction, etc., making the assumptions that the camera lenses have no aberrations and that the film planes are parallel to the front glass window of the chamber. These equations contain twelve constants whose direct measurement is difficult but whose physical significance is fairly clear. One can then make arguments

that certain terms in the equations relating X, Y, and Z to film measurements are small, where "small" is defined as being undetectable in terms of our measuring apparatus. Omitting these terms one can then finally write the following approximate stereographic reduction formulas:

$$X = x(P + QZ) + C_u QZ$$

$$Y = y(P + QZ) + C_v QZ$$

$$Z = \frac{-(y + y')P}{G + Q(y + y')}$$

where:

$P = 1.953$ $\qquad$ $C_u = -0.586$ cm

$Q = 0.0339$ cm^{-1} $\qquad$ $C_v = 3.005$ cm

$G = 0.2048$

and X, Y, Z, x, y, and y' are in centimeters. The values of the five constants are determined by making measurements on the images of points of known X, Y, and Z, i.e., grid marks on the front and back windows.

As mentioned earlier, X, Y, and Z are the coordinates of a point in real space. The coordinate system is defined as follows. The origin of the XYZ system is the central grid mark on the inside of the front window, the X axis is that axis of the fiducial mark system going in the direction of the incident beam, the Y axis is the vertical axis of the fiducial mark system, and the Z axis is the negative normal to this plane, directed to the back of the chamber. Note that this is a left-handed coordinate system.

The x, y, and y' refer to coordinates measured on the film negatives. On each film of the stereographic pair, the origin is taken to be the image of the origin of the XYZ system, i.e. the image of the central grid mark on the front glass window. The direction of the x axis for each film of the stereographic pair is taken as the direction of the

image of the X axis. The actual value of x for the image of a point in the chamber is the same (within experimental error) on each film of the stereographic pair, except in the infrequent cases of different film shrinkage. The direction of the y axis (on the lower film) and the y' axis (on the upper film) is perpendicular to the x axis. For illustration of this, see Figure 9.

To summarize these remarks, let us say that the coordinates of a point in real space were determined from measurements made on the film images of that point, by means of stereographic reduction formulas, which are approximate in the sense that they would not give exactly the correct values even if the measurements were made with complete precision.

Because of the basic random measurement errors discussed earlier, there will be errors in the corresponding values of X, Y, and Z. To find the effect of these errors, one uses the well-known equation of statistics for the standard deviation Δf of a function $\underline{f}$ in terms of the independent standard deviations Δx_i of the N independent variables x_i:

$$\Delta f = \left[\sum_{i=1}^{N} \left(\frac{\partial f}{\partial x_i} \Delta x_i \right)^2 \right]^{1/2}$$

Applying this to the equations for X, Y, and Z in terms of x, y, and y', we find:

$$\Delta X = \sqrt{(QZ + P)^2 (\Delta x)^2 + \frac{(x + C_H)^2 Q^2 P^2 G^2}{[Q(y + y') + G]^4} [(\Delta y)^2 + (\Delta y')^2]}$$

$$\Delta Y = \sqrt{\left\{(QZ + P) - \frac{PQG(C_V + y)}{[Q(y + y') + G]^2}\right\}^2 (\Delta y)^2 + \left\{\frac{PQG(C_V + y)}{[Q(y + y') + G]^2}\right\}^2 (\Delta y')^2}$$

$$\Delta Z = \frac{PG}{[G + Q(y + y')]^2} \sqrt{(\Delta y)^2 + (\Delta y')^2}$$

For the purposes of calculating the errors to be expected in a given event, the above formulas are too involved for practical use. Inserting the values of the constants P, Q, G, C_u, and C_v, one finds that the errors ΔX, ΔY, and ΔZ are essentially only functions of Δx, Δy, and $\Delta y'$, i.e., they are not rapidly varying functions of x, y, and y'. Utilizing this fact, one can write the errors in X, Y, and Z due to measurement errors as:

$$\Delta X \sim 2.2\, \Delta x$$

$$\Delta Y \sim 1.1 \sqrt{(\Delta y)^2 + (\Delta y')^2}$$

$$\Delta Z \sim 7.9 \sqrt{(\Delta y)^2 + (\Delta y')^2}$$

To give an idea of the magnitude of these errors, all double-V events were measured at least twice on different occasions; the average difference between pairs of measurements was:

$$\Delta X = 0.014 \text{ cm.}$$

$$\Delta Y = 0.011 \text{ cm.}$$

$$\Delta Z = 0.068 \text{ cm.}$$

In addition to these errors in X, Y, and Z due to random measurement errors, there are others which would still be present if $\Delta x = \Delta y = \Delta y' = 0$. These are due to the approximate nature of the camera formulas, and to the fact that the "constants" P, Q, G, C_u, and C_v could vary from picture to picture. Possible reasons for this might be:

a) different shrinkage of the two stereographic negatives due to different developing conditions;

b) local emulsion wandering due to lack of bonding between the emulsion and backing; and

c) local changes in the propane index of refraction arising from non-uniform temperature, producing visible heat wave.

The latter errors were about the same magnitude as the random errors; this was deduced by computing the real space coordinates of representative grid marks (from measurements made on their film images) and comparing them with their known values. This led to errors of:

$\Delta X \approx 0.02$ cm.

$\Delta Y \approx 0.02$ cm.

$\Delta Z \approx 0.15$ cm.

as the total error in the determination of true real-space coordinates due to systematic and random errors combined.

B. It will be remembered that the identification of events was based in part on the coplanarity of the production event. The production event was determined by the incident pion (traveling in the +X direction, with almost no Y or Z velocity component), the hyperon (Λ° or Σ^-) and the heavy meson (θ° or K^+). Errors in the coordinate measurements of points affected the precision of the coplanarity determination. If φ is the angle between the line A = 12 and the plane of B = 23 and C = 26, then:

$$\sin \varphi = \frac{\vec{A} \cdot \vec{B} \times \vec{C}}{|\vec{A}|\ |\vec{B}|\ |\vec{C}|}$$

For the production event, A is in the +X direction, so we have:

$$\sin \varphi = \frac{\vec{B} \times \vec{C}}{|\vec{B}|\ |\vec{C}|}$$

$$= \frac{(Y_3 - Y_2)(Z_6 - Z_2) - (Z_3 - Z_2)(Y_6 - Y_2)}{\sqrt{(X_3-X_2)^2+ (Y_3-Y_2)^2+ (Z_3-Z_2)^2}\ \sqrt{(X_6-X_2)^2+ (Y_6-Y_2)^2+ (Z_6-Z_2)^2}}$$

In theory one could now differentiate this with respect to X_2, X_3, X_6, Y_2, Y_3,...., and calculate the error:

$$\Delta\varphi = \left(\frac{\partial\varphi}{\partial X_2}\Delta X_2\right)^2 + \left(\frac{\partial\varphi}{\partial X_3}\Delta X_3\right)^2 + \cdots$$

Clearly it would be tedious to calculate this for each event. One can, however, perform the indicated differentiations and find out in what quantities the main dependence lies. If one does this one finds a crude measure of the error $\Delta\varphi$ to be expected in coplanarity is (for φ near 0°):

$$\Delta\varphi = \Delta X/R$$

where $\Delta\varphi$ is in radians, ΔX is an average coordinate error (usually taken as 0.1 cm), and R is the length of the shortest track used in defining the plane. This expression also served to estimate the expected error in determining the coplanarity of decay planes. For the double-V events, where coplanarity played an important role, all events were measured at least twice to get some direct idea of the coplanarity errors.

C. In addition to coplanarity of the production event (and of the decay event, for Λ° - θ° and Σ° - θ° reactions) it will be remembered that the production angles θ_{123} and θ_{126} (see Fig. 9) were used, as well as the decay angles. Since the decay angles were important in identifying Λ° - θ° and Σ° - θ° events, and since calculation of the error in decay angles due to measurement errors was difficult, these events were all measured at least twice to give some direct idea of the error.

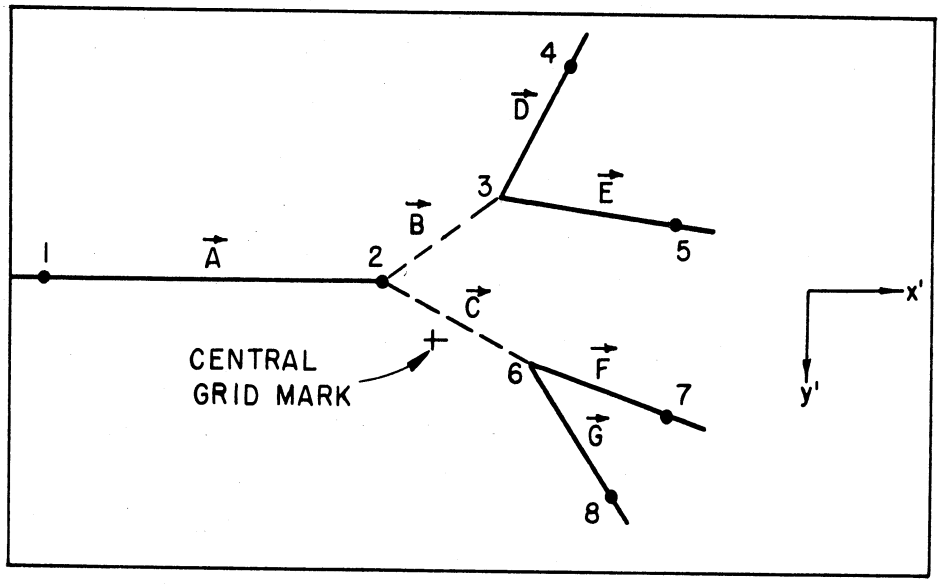

TOP CAMERA VIEW

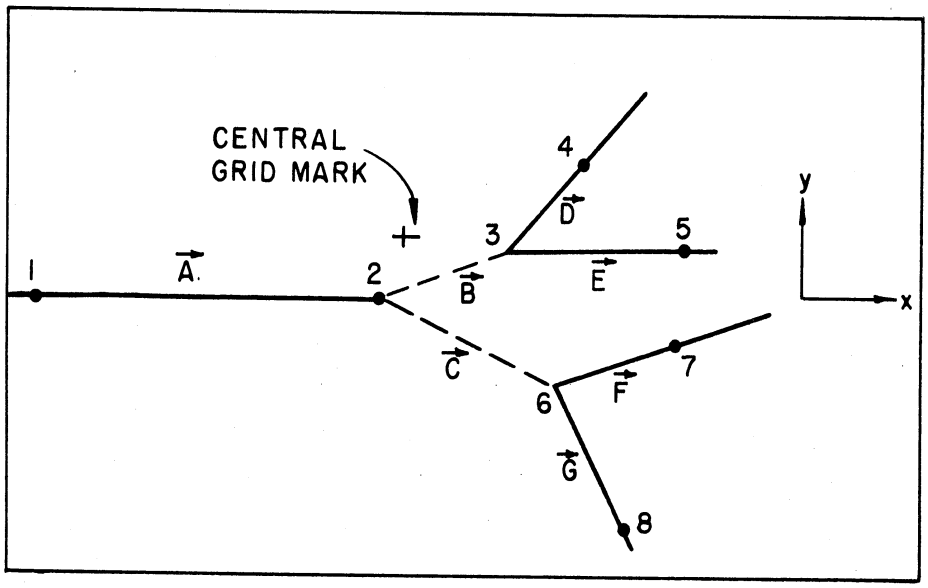

BOTTOM CAMERA VIEW

Figure 9. Double V Event As Seen On Film

For the production event, however, the angular errors could be approximately calculated. We note for example:

$$\cos \theta_{123} = \frac{\vec{A} \times \vec{B}}{|\vec{A}| \, |\vec{B}|}$$

which gives as a sample error component (due to ΔY_3):

$$\frac{\Delta \cos \theta_{123}}{\cos \theta_{123}} \approx - \frac{(Y_3 - Y_2)}{|\vec{B}|^2} \sin \alpha \cdot \Delta Y_3$$

where α is the angle between the production plane and the X-Y plane.

One error in particular was of some importance in the double-V events. This arose from the uncertainty in X_2 (the X coordinate of the incident pion ending) because of the finite bubble density. Assuming an average bubble density of about 15 bubbles per centimeter, then the value of X_2 could be increased by 1/30 cm on the average. This affected the angle θ as follows:

$$\Delta \cos \theta_{123} = \frac{\sin^2 \theta_{123}}{|\vec{B}|} \Delta X_2$$

or

$$\Delta \theta_{123} = \frac{\sin \theta_{123}}{|\vec{B}|} \Delta X_2$$

If $\theta_{123} = 30°$, $|\vec{B}| = 1$ cm, $\Delta X_2 = 1/15$ cm, then $\Delta\theta_{123} \sim 2°$.

Another inherent error in determining angles arose from the Coulomb scattering which is noticeable on slow tracks. This could be partially compensated for by careful selection of points to be measured.

3.5.3 Momentum Errors

Another of the criteria used in identifying double-V events was that of calculating the strange particle momentum from the decay angles.

Clearly it would be desirable to have the momentum errors resulting from angular errors as small as possible in order to have the momentum equality criterion be a sharp one. Unfortunately this was not always the case.

Consider first the momentum deduced from the decay. Figure 10 shows the graph used to determine the momentum of a Λ° knowing θ_p (the laboratory angle of the decay proton with respect to the Λ° line of flight) and θ_π (the laboratory angle of the decay pion with respect to the Λ° line of flight). It is clear just by inspection that for high Λ° momenta a small change in angle produces a large change in momentum. Figure 11 shows the analogous graph for the Θ° decay; here the dependence on angle is not quite so serious.

The momentum deduced from production also depends on angular errors in θ_Λ (the laboratory angle between the Λ° and the incident π^-) and θ_Θ (the laboratory angle between the Θ° and the incident π^-). Figures 12 and 13 show the momentum dependence as a function of θ_Λ and θ_Θ; errors here were in general smaller than those involved in the momentum determination from the decay.

3.5.4 Identification Errors

We now ask ourselves the following question: "As a result of all the errors just discussed, how many events were incorrectly identified?" An event was classified as being a certain type ($\Sigma^- - K^+$, $\Lambda^\circ - \Theta^\circ$, or $\Sigma^\circ - \Theta^\circ$) if it could satisfy all the criteria of that type. An event which, measured with complete precision, would not have satisfied the criteria, might have satisfied all the criteria consistent with the various expected errors. We must now estimate the number of such "false coincidences."

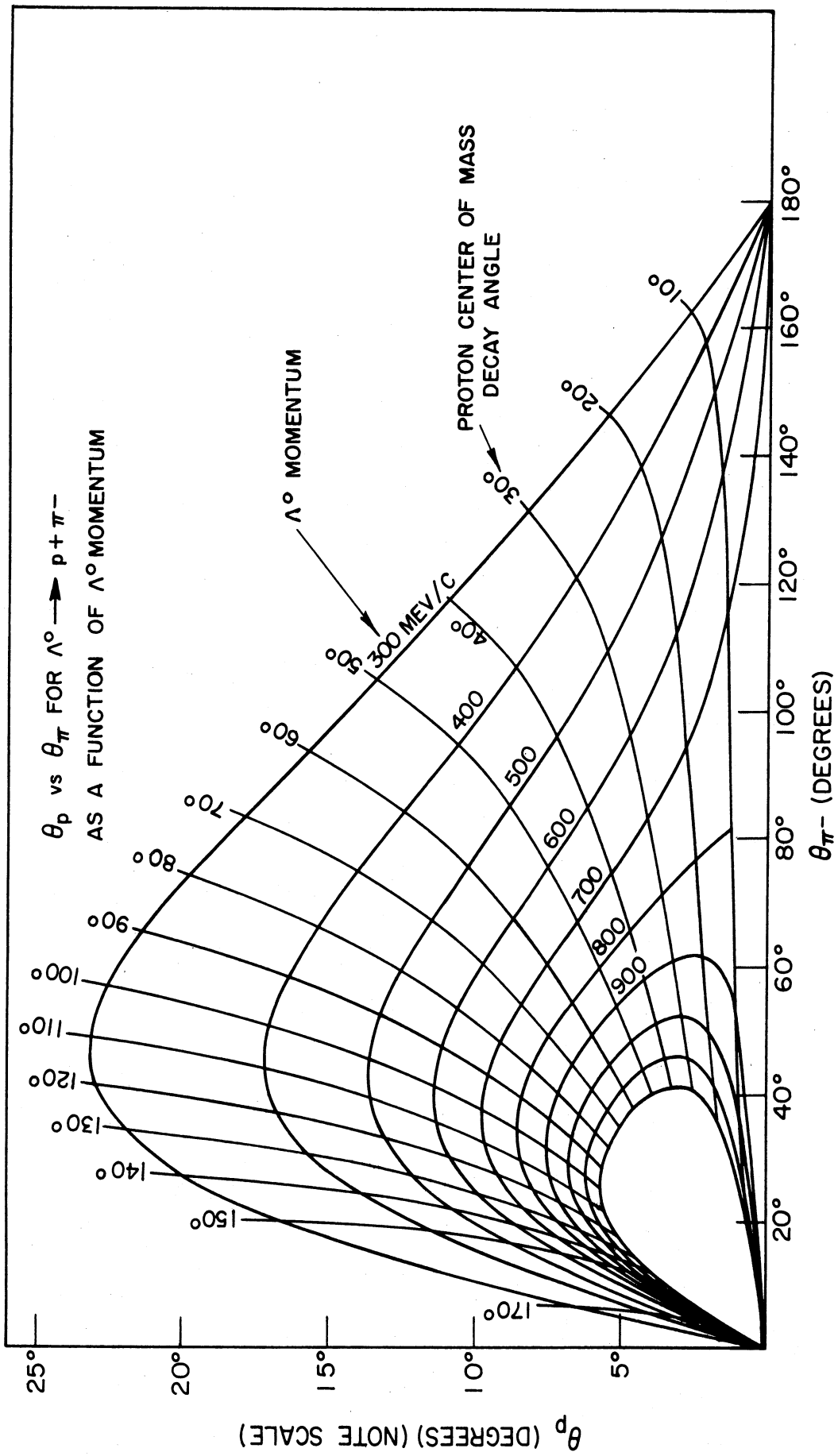

Figure 10. Graph of θ_p vs. θ_π for Λ° Decay

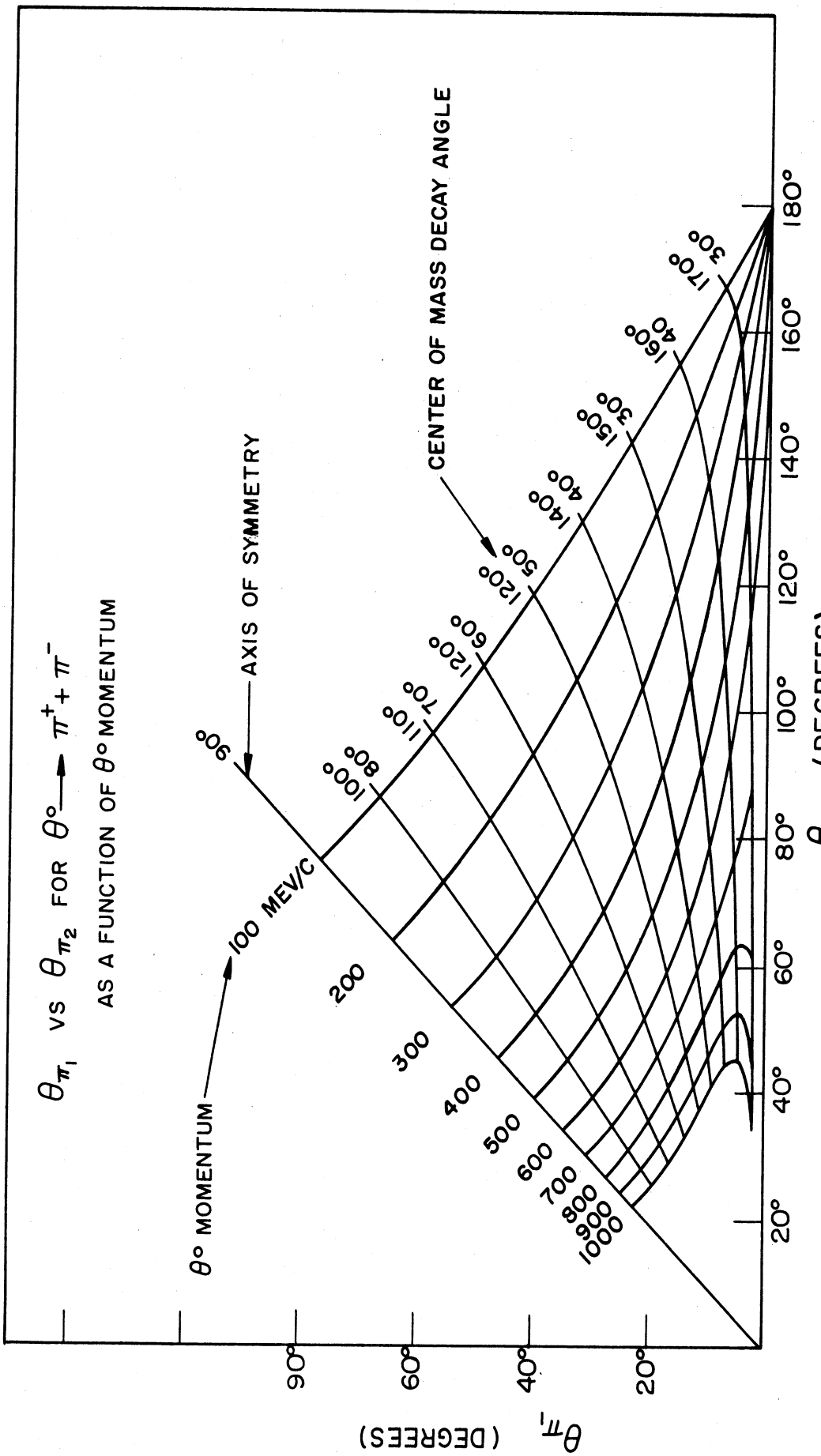

Figure 11. Graph of θ_{π_1} vs. θ_{π_2} for $\theta°$ Decay

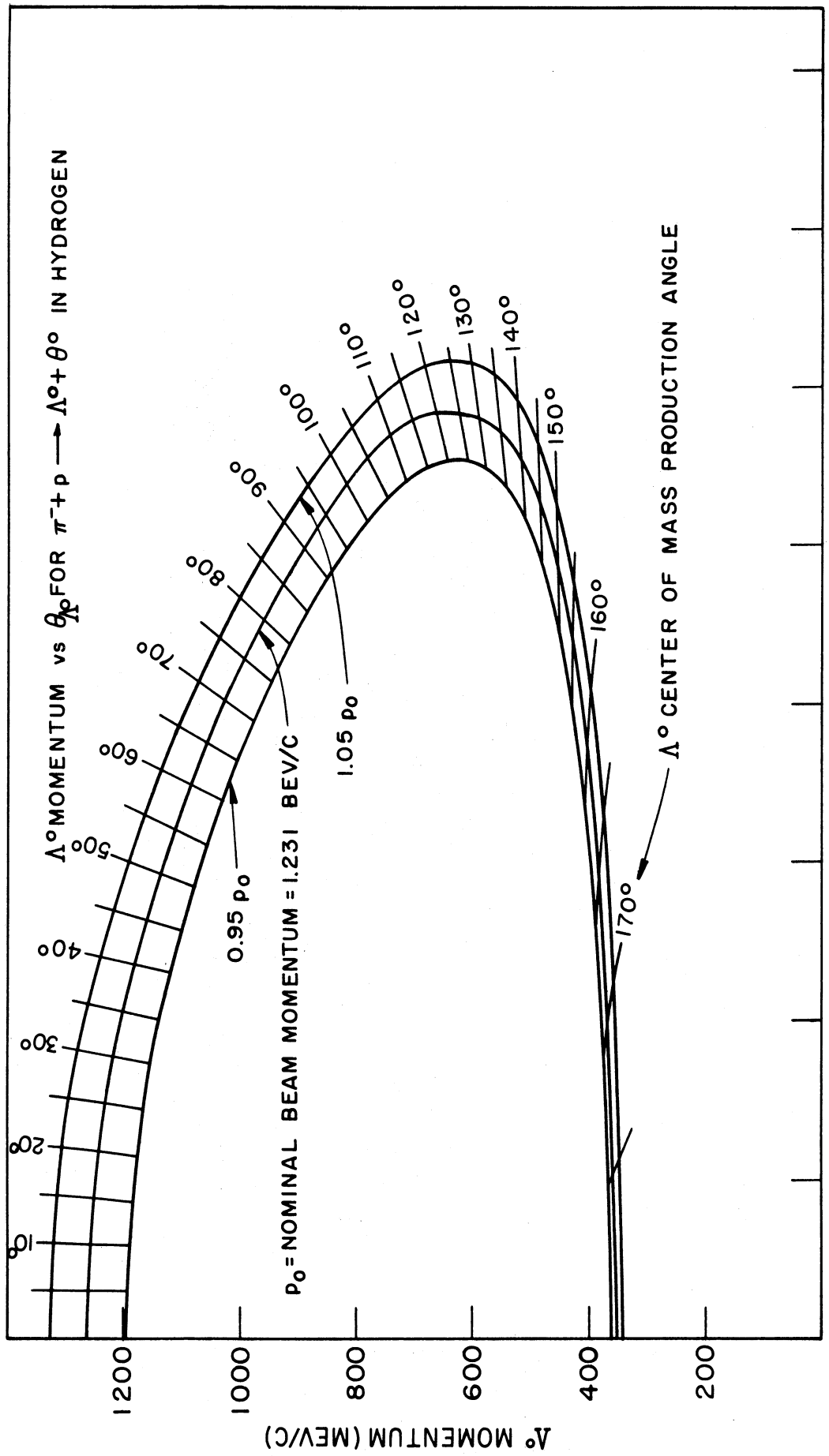

Figure 12. Momentum of Λ° vs. θ_Λ for Reaction $\pi^- + p \rightarrow \Lambda^\circ + \theta^\circ$

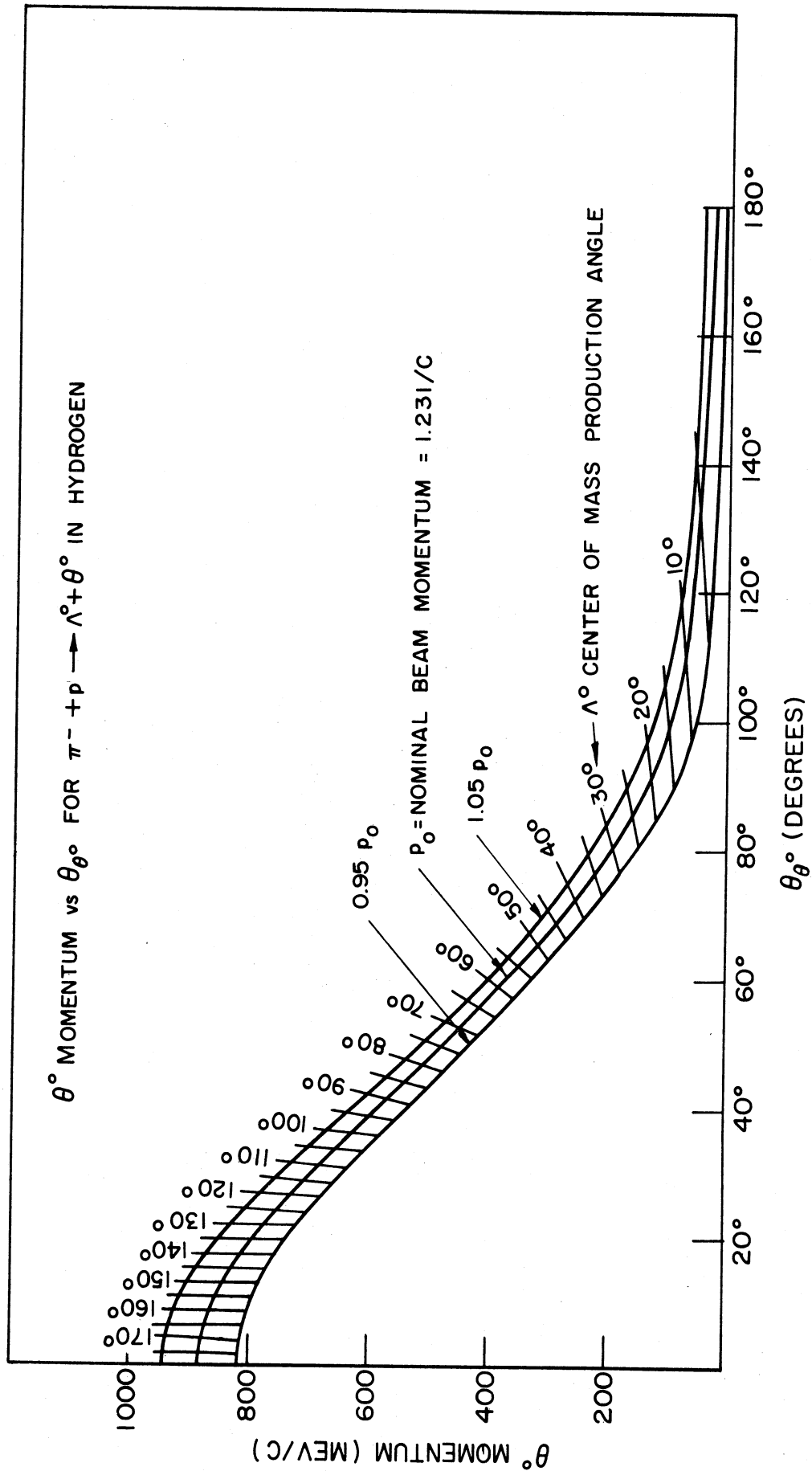

Figure 13. Momentum of θ° vs. θ_θ for Reaction $\pi^- + p \rightarrow \Lambda^\circ + \theta^\circ$

We consider first the Σ^- - K^+ events; the criteria to be satisfied were:

1) agreement of θ_{Σ^-} and θ_{K^+} with predicted ranges of values;

2) agreement of range and bubble density; and

3) coplanarity of production event.

On a graph like that in Fig. 4 were plotted all events which were consistent with coplanarity within the expected error (there were approximately 130 such events). Some of these fell within the predicted range of θ_Σ - θ_K values, while the rest (about 80) did not, forming a background of non-Σ^- - K^+ events. By looking at this background one could estimate by extrapolation that perhaps 5 non-Σ^- - K^+ events would have fallen by chance with the acceptance region. At least half of these, however, would have been discarded by bubble density and range criteria. Thus we concluded that not more than 2 or 3 events of the 51 Σ^- - K^+ events were incorrectly identified.

One can estimate the number of falsely identified Σ^- - K^+ events by another method (11). A fundamental hypothesis of this method is that all false events are Σ^- - K^+ events occurring in carbon. This is quite likely to be true since bubble density would serve to rule out many of the other categories. One then calculates the kinematics of carbon events for selected values of struck proton momentum, angle between pion and proton momenta, and center of mass production angle. One assumes the carbon center of mass production angular distribution to be the same as that in hydrogen. One further assumes that for propane the total carbon cross section is 1.5 times the total hydrogen cross section (12) and that half the carbon events would be immediately

rejected because of the presence of recoil prongs at the point of production. Using these assumptions and the following criteria:

1) agreement of θ_Σ and θ_K with hydrogen values,

2) agreement of range, and

3) coplanarity less than 3°,

one can proceed to calculate how many events claimed to be hydrogen were actually carbon events which satisfied the hydrogen criteria within acceptable limits.

The number of such events for each of the center of mass production quadrants is shown in Table 4. Under each quadrant heading is shown the number of events originally claimed to be hydrogen; in the table are the numbers of these which could actually have been carbon. We note that, using all the criteria, only one event out of the total of 51 Σ^- - K^+ events is likely to be carbon; this compares with the estimate from background events of 2 or 3.

Gross errors in measuring, card punching, computing, etc., could have caused genuine hydrogen Σ^- - K^+ events to be discarded. Great care was taken to see that this did not happen; in approximately 50 V° events which were measured two or more times no inconsistencies outside measuring errors were found. It is unlikely that more than 1 or 2 hydrogen events were discarded.

TABLE 3. NUMBER OF EVENTS IN OBSERVED SAMPLE OF "HYDROGEN" Σ^- - K^+ EVENTS WHICH WERE PROBABLY PRODUCED IN CARBON

Criteria Used	Center-of-Mass Production Angle				
	0-60° (23)	60°-90° (17)	90°-120° (10)	120°-180° (1)	Total (51)
I	2.3	2.0	1.2	0.1	5.6
I+II	0.5	1.3	1.1	0.1	3.0
I+II+III	0.3	0.4	0.3	0.0	1.0

We consider next identification errors in hydrogen Λ° - θ° events. The only feasible method of calculating the number of falsely identified events is to use the theoretically calculated values as outlined in the discussion of Σ^- - K^+ events. The same assumptions were made, only here there are three possible sources of contamination:

$$\pi^- + p \rightarrow \Lambda^\circ + \theta^\circ \text{ in carbon}$$

$$\pi^- + p \rightarrow \Sigma^\circ + \theta^\circ \text{ in carbon}$$

$$\pi^- + p \rightarrow \Sigma^\circ + \theta^\circ \text{ in hydrogen}$$

The contamination from the last category is hard to estimate but is certainly less than 6% of the total. Contributions from the first category were tested by the following two criteria:

1) agreement of θ_{Λ° and θ_{θ° with hydrogen values within acceptable limits, and

2) coplanarity less than 3°.

The contributions from Λ° - θ° events in carbon under these restrictions are shown in Table 5.

TABLE 4. NUMBER OF EVENTS IN OBSERVED SAMPLE OF "HYDROGEN"

$\Lambda^\circ - \theta^\circ$ EVENTS WHICH WERE PROBABLY $\Lambda^\circ - \theta^\circ$ EVENTS IN CARBON

Criteria Used	Center-of-Mass Production Angle				
	0°-60° (0)	60°-90° (1)	90°-120° (3)	120°-180° (11)	Total (15)
I	--	0.1	0.2	0.7	1.0
I + II	--	0.0	0.1	0.4	0.5

Contributions from $\Sigma^\circ - \theta^\circ$ events in carbon were tested by two criteria:

1) agreement of θ° momentum at given θ° angle with value predicted by hydrogen kinematics, and

2) coplanarity less than 3°;

the results are listed in Table 6. Probably the numbers quoted are too high, due to the lack of criteria which can easily be applied. The total contamination due to $\Sigma^\circ - \theta^\circ$ events in carbon is probably no greater than that due to $\Lambda^\circ - \theta^\circ$ events in carbon.

TABLE 5. NUMBER OF EVENTS IN OBSERVED SAMPLE OF "HYDROGEN"

$\Lambda^\circ - \theta^\circ$ EVENTS WHICH WERE PROBABLY $\Sigma^\circ - \theta^\circ$ EVENTS IN CARBON

Criteria Used	Center-of-Mass Production Angle				
	0°-60° (0)	60°-90° (1)	90°-120° (3)	120°-180° (11)	Total (15)
I	--	0.2	0.4	2.2	2.8
I + II	--	0.1	0.2	0.9	1.2

Finally we consider the number of falsely identified hydrogen $\Sigma^\circ - \theta^\circ$ events. The two sources of contamination are $\Sigma^\circ - \theta^\circ$ and $\Lambda^\circ - \theta^\circ$ events in carbon; the two sets of criteria are:

1) agreement of θ° momentum at given θ° angle with hydrogen value;

2) reasonable value of Σ° momentum; and

3) coplanarity less than 5.75°;

and

1) agreement of θ° momentum at given θ° angle;

2) coplanarity less than 5.75°; and

3) reasonable value of Λ° momentum.

The results are displayed in Tables 7 and 8, respectively.

TABLE 6. NUMBER OF EVENTS IN OBSERVED SAMPLE OF "HYDROGEN" $\Sigma^\circ - \theta^\circ$ EVENTS WHICH WERE PROBABLY $\Sigma^\circ - \theta^\circ$ EVENTS IN CARBON

Criteria Used	Center-of-Mass Production Angle				
	0°-60° (2)	60°-90° (1)	90°-120° (3)	120°-180° (8)	Total (14)
I	0.3	0.2	0.7	2.4	3.6
I+II	0.3	0.2	0.6	2.0	3.1
I+II+III	0.2	0.1	0.5	1.7	2.5

TABLE 7. NUMBER OF EVENTS IN OBSERVED SAMPLE OF "HYDROGEN" $\Sigma^\circ - \theta^\circ$ EVENTS WHICH WERE PROBABLY $\Lambda^\circ - \theta^\circ$ EVENTS IN CARBON

Criteria Used	Center-of-Mass Production Angle				
	0°-60° (2)	60°-90° (1)	90°-120° (3)	120°-180° (8)	Total (14)
I	0.3	0.2	0.6	1.2	2.3
I+II	0.3	0.2	0.4	1.0	1.9
I+II+III	0.3	0.2	0.3	0.7	1.5

3.6 Scanning Efficiency and Biases

In discussing total or differential production cross sections or angular distributions of decay, certain biases and scanning efficiencies must be taken into account. In a well-planned experiment, only those events which could be detected with high efficiency (or a small bias) would be considered. If that were done in this case, the number of events would be vanishingly small. For that reason, all events found whether efficiently scanned or not were included in the results. This necessitates evaluating all biases and efficiencies with the least possible error. In the following paragraphs the importance of each effect will be denoted by a factor by which the observed cross section must be multiplied to allow for the effect. Finally all the various factors will be multiplied together to obtain the corrected cross section.

Several effects immediately suggest themselves. One is due to the attenuation of the pion beam in passing through the chamber. Since the number of pion tracks was counted as the beam entered the chamber, and since some pions were lost in interactions not producing strange particles, the number of effective pions was overestimated. The factor for this effect was 1.12, with negligible errors. One should also include a factor of 1.08 to allow for μ contamination of the beam.

A second effect arose from lowered detection efficiency near the windows, the top and the bottom of the chamber, where events did not take place entirely in the visible volume. The factor for this effect was 1.04; in general, this effect could be eliminated by better beam collimation.

A third effect is that due to what one would normally call scan-

ning efficiency. It was obvious that in scanning for an event as rare as strange particle production one could not be 100% efficient if a finite time was spent on scanning.

For $\Sigma^- - K^+$ events, the following method was used to evaluate the scanning efficiency. Upon plotting the distribution along the beam direction (the X axis) of real (or apparent) $\Sigma^- - K^+$ events, the results shown in Fig. 14 were obtained. The dotted line represents a least squares fit by a straight line to the number of events observed in the central region of the chamber (-12 cm $\leq X \leq +12$ cm). The small number of events in the first 3 cm of the chamber was due to difficulty in picking up pion tracks just as they entered the chamber. The lack of any events in the last 3 cm ($+12$ cm $< X \leq +15$ cm) is due to the fact that Σ^-'s or K^+'s produced in this interval would escape out the end of the chamber before undergoing an identifying decay.

One is tempted to ascribe the sloping line in the center of the chamber to a sort of "reading effect". When scanning along any given pion track one's interest and attentiveness decrease as one gets further and further along the track. This may be due in part to the increasing background of tracks resulting from scatterings, etc., in the front part of the chamber, and in part to the fallacious subconscious assumption that the probability of an event occurring decreases the further a given pion goes without interacting.

Since one would expect the distribution of $\Sigma^- - K^+$ events to be constant as a function of X (except for a slight beam attenuation), one is led to say that the scanning efficiency is not constant throughout the chamber. Assuming that the efficiency is 100% for X = 12 cm and that it decreases linearly (as indicated by the dotted line) for -12 cm $< X +$ 12 cm, and is zero for $+12$ cm $< X \leq +15$ cm (which allows in a crude way for

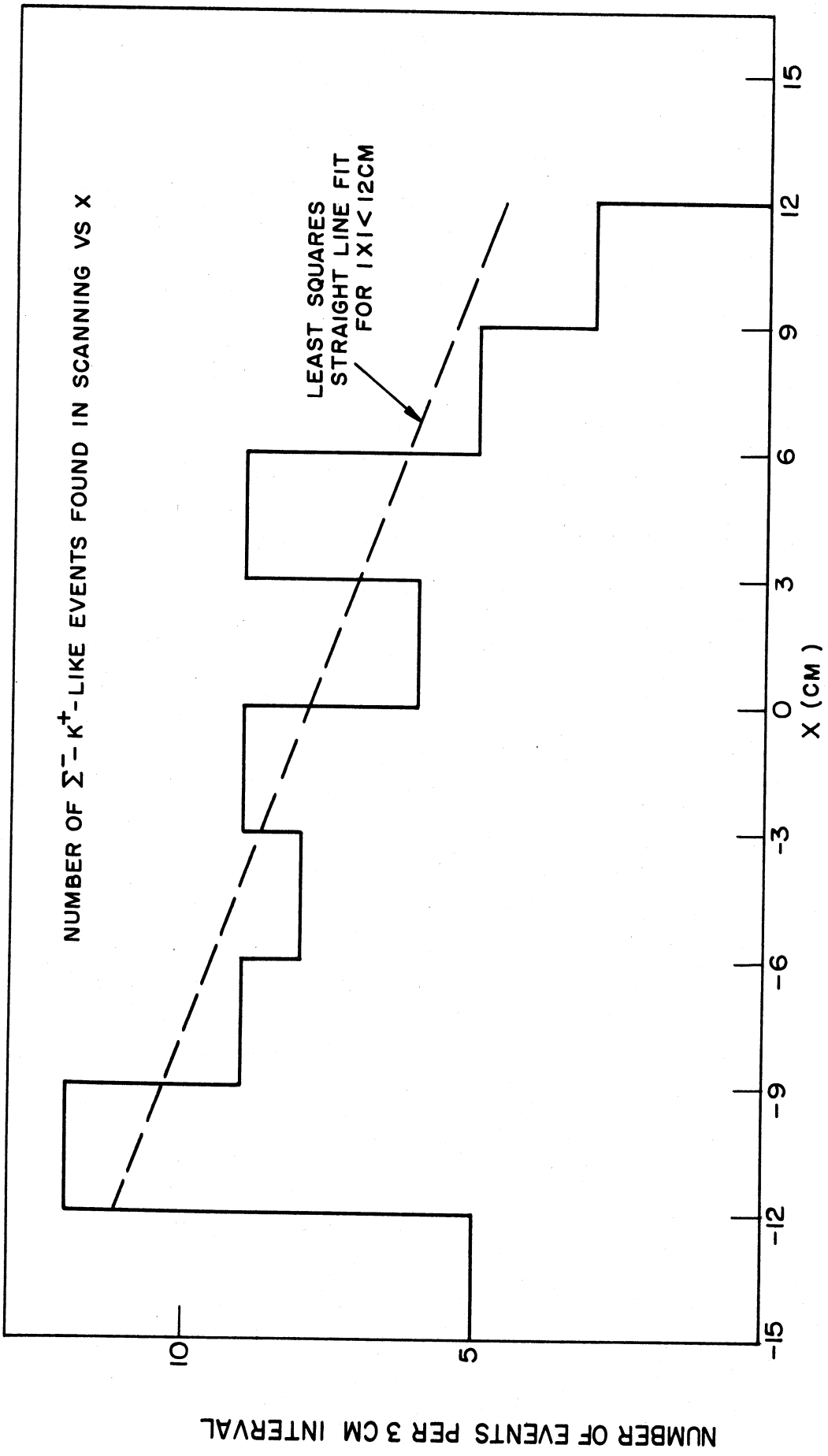

Figure 14. Distribution of Apparent Σ^- - K^+ Events as Function of X

escapes out the end), one can calculate the average scanning efficiency. The factor for this effect determined in this fashion is 1.48 ± 0.20.

An alternative method of checking scanning efficiency, used for neutral V events, is multiple scanning. Such a method, however, usually has implicit in it the assumptions that the scanners' efficiencies are constant and independent. Neither of these is necessarily true; the scanners' effort varies from day to day, and all scanners tend to pick up "easy" events and miss "hard" ones. An analysis of single V scanning efficiency was made by rescanning, with the result that the efficiency was about 68%. Extrapolating this to double-V events by knowing the efficiency for picking up the second V once the first was found led to difficulties, however, due to the fact that the scanning efficiency for an event cannot be expressed as the product of the scanning efficiencies for the several parts. Attempts to do so led to contradictions, e.g., the scanning efficiency for π track endings being greater than 100%. Reconciling rescanning results as much as possible, the factor for scanning efficiency in double-V events was taken as 1.54 ± 0.20.

Further corrections include bias against seeing events with very short tracks in them. Analysis of events in a number of experiments indicated that the detection efficiency for tracks with a real-space length of less than about 0.4 cm is poor; we assumed it to be zero as the simplest approximation. In $\Sigma^- - K^+$ events, either the Σ^- or K^+ can have a short track. For center of mass production angles less than 15°, the K^+ range is less than 0.4 cm. Extrapolating the observed distribution to 0°, one finds a factor of 1.01. Short Σ^- ranges can result from

decays in flight near the point of production. One calculates a factor of 1.05 (from the momentum distribution and lifetime) for this correction.

A bias also existed against events involving small angles of decay of the Σ^-. The minimum detectable angle was unknown, but was less than 10°. Knowing the observed laboratory decay angular distribution we calculated a factor of 1.02 for this effect.

In neutral V decays, corrections had to be added to allow for short ranges of the decay products. For θ^0's this factor was 1.02; for Λ^0's, it was 1.07. For the Σ^- events, this correction did not occur, since the range of the decay pion was always greater than 1 cm.

TABLE 8. SUMMARY OF BIAS, EFFICIENCY FACTORS

Factor	$\Sigma^- - K^+$	V°
Beam attenuation	1.12	1.12
Muon contamination	1.08	1.08
Scanner's "efficiency"	1.48 ± 0.20	1.54 ± 0.20
Edge effect	1.04	1.04
Short Σ^- track	1.05	--
Short K^+ track	1.01	--
Small Σ^- decay angle	1.02	--
Short decay product range	1.00	1.09
Total correction	2.01 ± 0.27	2.10 ± 0.27

All the various factors are collected in Table 8. It is obvious that some factors are negligible; they were included because the question of their relative importance comes to mind immediately. There are a great many other small effects which were not included because they would not affect the conclusions appreciably.

IV. EXPERIMENTAL RESULTS AND THEIR INTERPRETATION

4.1 Total and Differential Production Cross Sections

4.1.1 Σ^- - K^+ Production

A total of 51 events was found which were interpreted to be examples of the reaction $\pi^- + p \rightarrow \Sigma^- + K^+$ occurring in hydrogen. On the basis of the discussion in Chapter III, a very small number may possibly be carbon events. These 51 events were distributed according to center of mass production angle as shown in Fig. 15.

On the basis of 41 events found in approximately 80% of the total number of pictures (the rest not being included because of their poor quality) the uncorrected total cross section was 0.10 mb. Multiplying by the factor 2.01 ± 0.27 to allow for scanning biases and by a factor of 0.96 ± 0.03 to account for probable carbon contamination we find a total corrected cross section of 0.19 ± 0.05 mb.

Initially the error calculated was a standard deviation formed by assuming all quantities to be normally distributed. This is certainly not the case (e.g., the cross section has a Poisson distribution) and for this reason the error quoted here has been increased slightly over the value computed by the above method. The small number of observed events and the uncertainty in the scanning efficiency contribute about equally to the quoted error.

4.1.2 Λ° - θ° Production

A total of 15 events was found which were interpreted to be examples of the reaction $\pi^- + p \rightarrow \Lambda^\circ + \theta^\circ$ occurring in hydrogen, where both strange particles were observed to decay via the charged mode. The center of mass angular distribution of production is shown in Fig. 16.

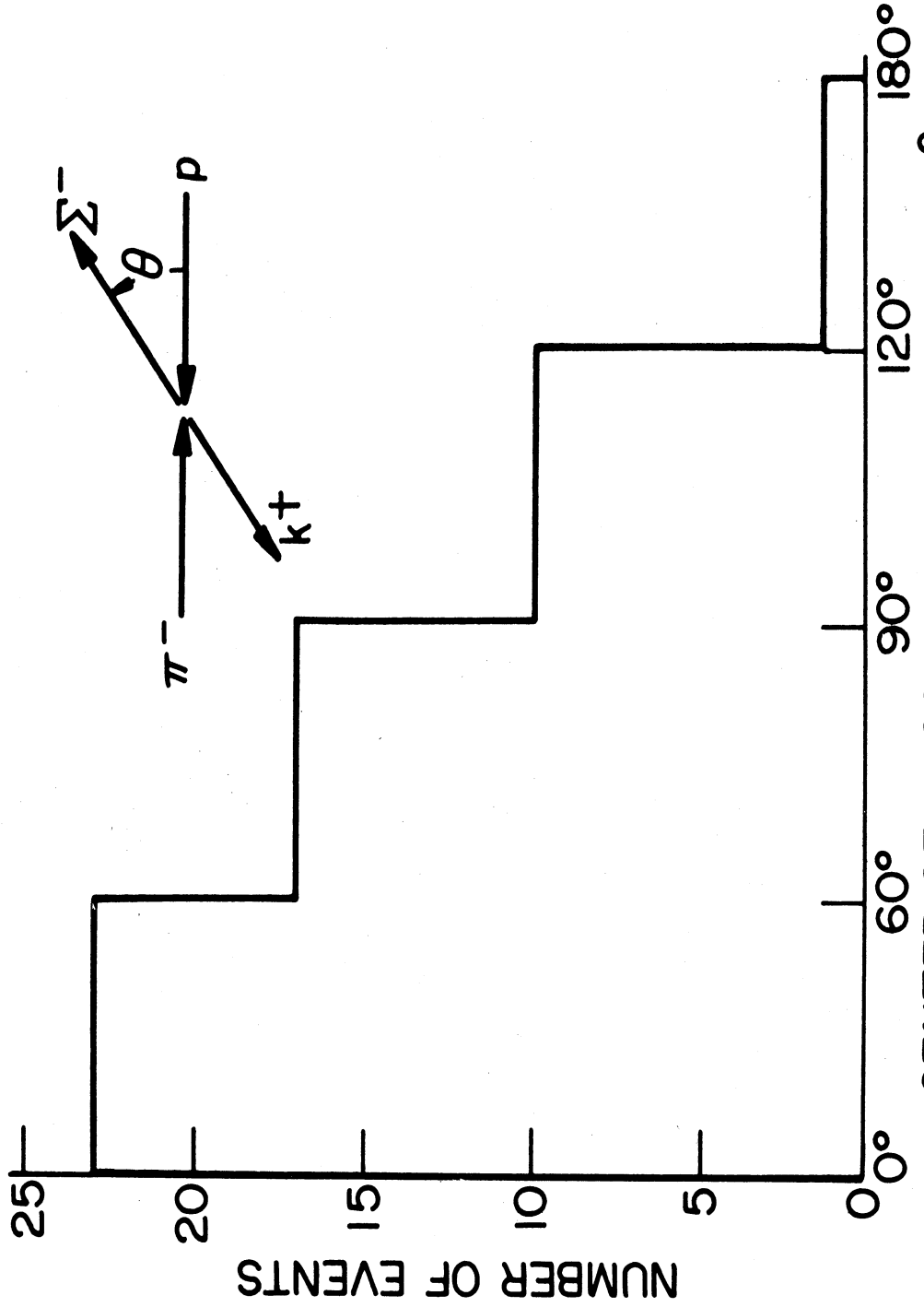

Figure 15. Production Angular Distribution for Reaction $\pi^- + p \rightarrow \Sigma^- + K^+$

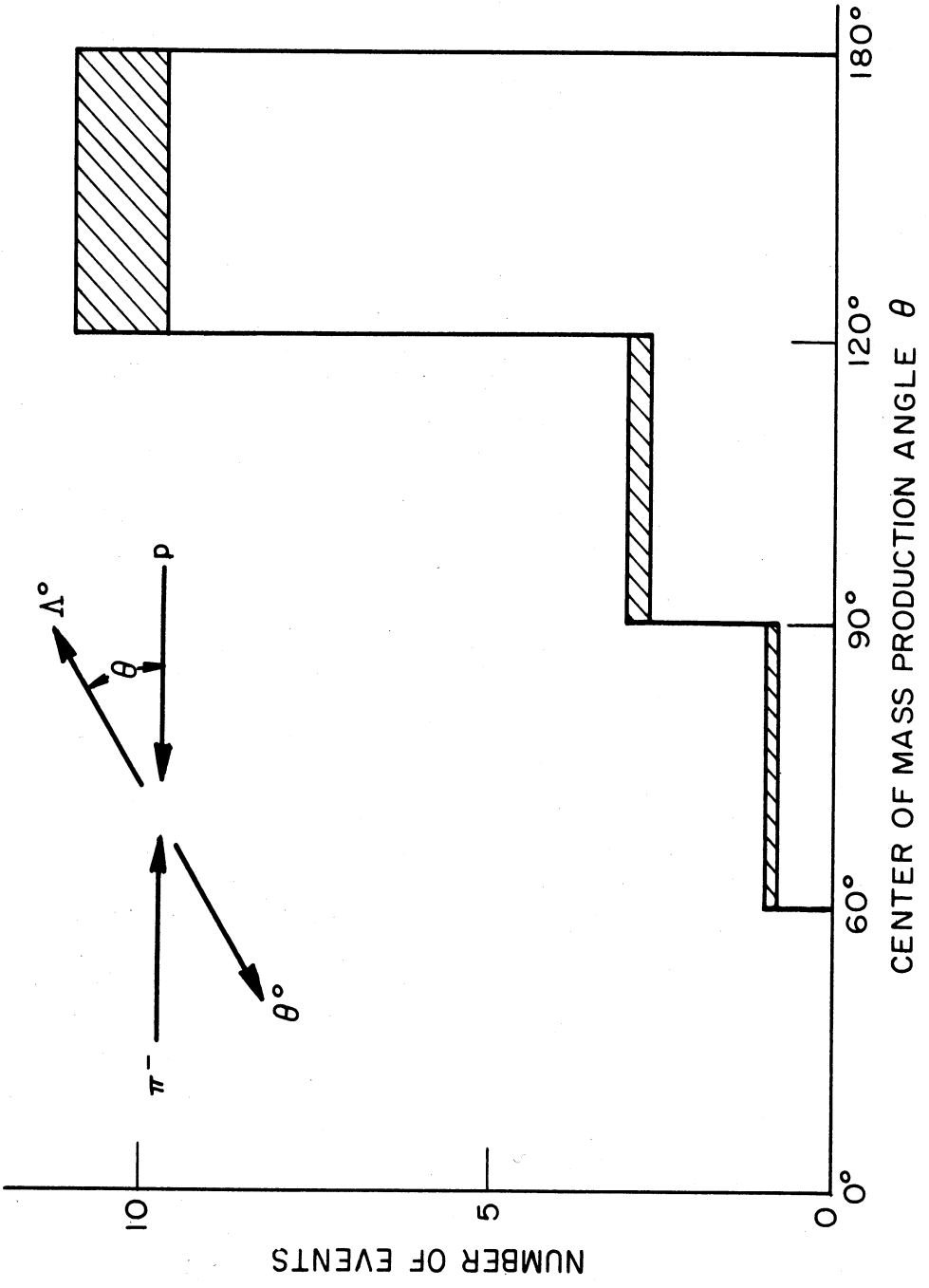

Figure 16. Production Angular Distribution for Reaction $\pi^- + p \rightarrow \Lambda^\circ + \theta^\circ$

The shaded portions represent the events which could reasonably be carbon events.

To calculate the total cross section for Λ° - θ° production in hydrogen (including neutral decay modes) one must multiply the observed cross section of 0.03 mb by three factors:

1) 2.10 ± 0.27 to allow for scanning biases,

2) 0.93 ± 0.07 to allow for carbon contamination,

3) 1.47 ± 0.10 to allow for neutral decay modes of the Λ°, and

2.38 ± 0.30 to allow for neutral decay modes of the θ° (13),

which gives as the total production cross section 0.24 $\pm$ 0.09 mb.

4.1.3 Σ° - θ° Production

Fourteen events were observed which were interpreted as $\pi^- + p \rightarrow \Sigma^\circ + \theta^\circ$ occurring in hydrogen. To obtain the total production cross section one must use the following multiplying factors:

1) 2.10 ± 0.27 for scanning biases,

2) 0.71 ± 0.15 for carbon contamination, and

3) 1.47 ± 0.10 and 2.38 ± 0.30 for neutral decay modes,

giving 0.17 $\pm$ 0.07 mb as the total production cross section. The center of mass production angular distribution is shown in Fig. 17. The largest source of error in both the Λ° - θ° and Σ° - θ° total production cross sections is the small number of events. The cross sections also depend quite critically on the values of the carbon contamination and the escape coefficients.

4.2 Lifetimes of the Σ^-, Λ°, and θ°

Since the momenta of the various strange particles in each event are known, one can calculate the time elapsed, t_i, before each decay. Knowing also the coordinates in the chamber of each event, one can also

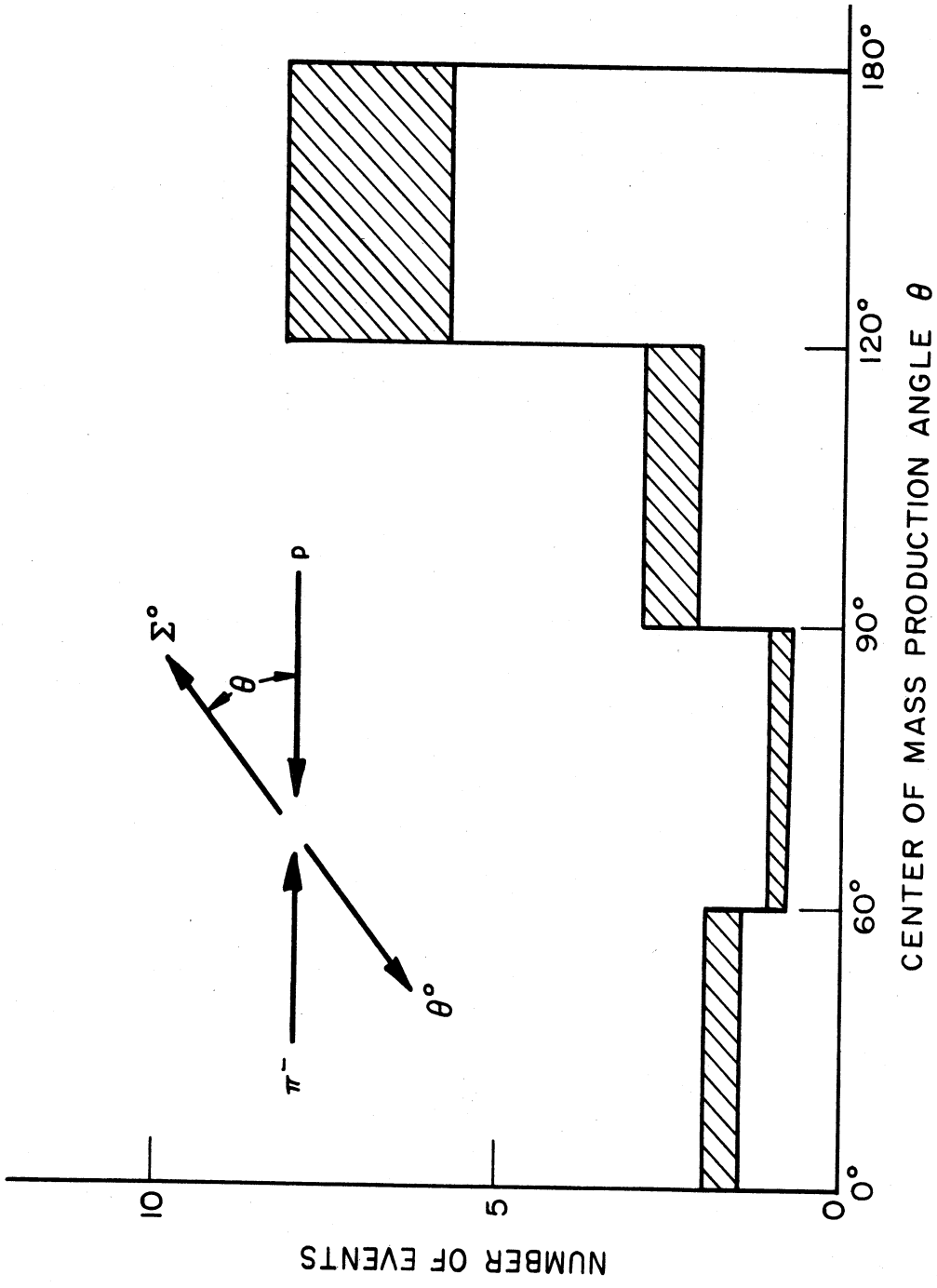

Figure 17. Production Angular Distribution for Reaction $\pi^- + p \rightarrow \Sigma^\circ + \theta^\circ$

calculate the potential time, T_i, each particle could have lived and still have had a decay visible in the chamber. Attempting to fit a simple exponential to the observed distribution of elapsed decay times will not give the correct lifetime, because one is limited by the finite size of the chamber to a certain restricted interval of decay times.

It is fruitful instead to use the statistical tool known as the "maximum likelihood method" (14). One writes as the probability distribution for a particle of lifetime τ decaying in an interval dt_i about the time t_i when the potential time available is T_i:

$$f(\tau;\, t_i, T_i) \;=\; \frac{e^{-t_i/\tau}}{1 - e^{-T_i/\tau}} \cdot \frac{dt_i}{\tau}$$

Since all events are independent, the probability of getting the total set of observed values of t_i and T_i (as a function of τ) is simply the product of the separate probabilities, and is known as the likelihood function:

$$L(\tau;\, t_i, T_i) \;=\; \prod_{i=1}^{N} \frac{e^{-t_i/\tau}}{1 - e^{-T_i/\tau}} \cdot \frac{1}{\tau}$$

This is a function of the experimental data (t_i, T_i) and the unknown lifetime τ. To find the most likely value of the lifetime τ one simply differentiates the above equation, sets the result equal to zero and solves for the lifetime τ. To find the probability relative to this maximum value for other values of τ one uses the original likelihood function.

Simply as a computational aid, one makes certain manipulations and approximations in the above formulas and defines a certain function $S'(1/\tau)$. This function has the following properties: the most probable value of $1/\tau$ is given by $S'(1/\tau) = 0$; the value of S' for a given value of τ represents the number of standard deviations away from the mean

which that particular value of τ is. Tables are then prepared giving S' as a function of the observed data (t_i, T_i) and the lifetime. Results computed by this method are:

$$\tau(\Sigma^-) = 1.67\ ^{+0.40}_{-0.28} \times 10^{-10} \text{ sec}$$

$$\tau(\Lambda^\circ) = 2.24\ ^{+0.79}_{-0.48} \times 10^{-10} \text{ sec}$$

$$\tau(\theta^\circ) = 0.74\ ^{+0.21}_{-0.15} \times 10^{-10} \text{ sec}$$

Errors quoted represent 63% confidence limits. A graph of the S' functions is shown in Fig. 18.

Unknown scanning biases and the use of approximation formulas will tend to affect the mean value slightly. The largest source of error is the small number of events. Uncertainties in the experimental quantities t_i and T_i contribute negligibly to the error.

A word of caution should be inserted here on the use of the S' function. For values of the lifetime within two standard deviations of the mean the S' function gives very nearly the same results as the exact likelihood function; for values farther from the mean, however, the S' function assigns too small a probability, i.e., such extreme values are more probable than the S' function would indicate.

The lifetimes quoted above are in reasonable agreement with results from other experiments. Really definitive lifetimes perhaps await the use of counter techniques.

4.3 Decay Angular Distributions

Two observable angular distributions relating to the decay of the Σ^-, Λ°, and θ° which have some theoretical significance are described

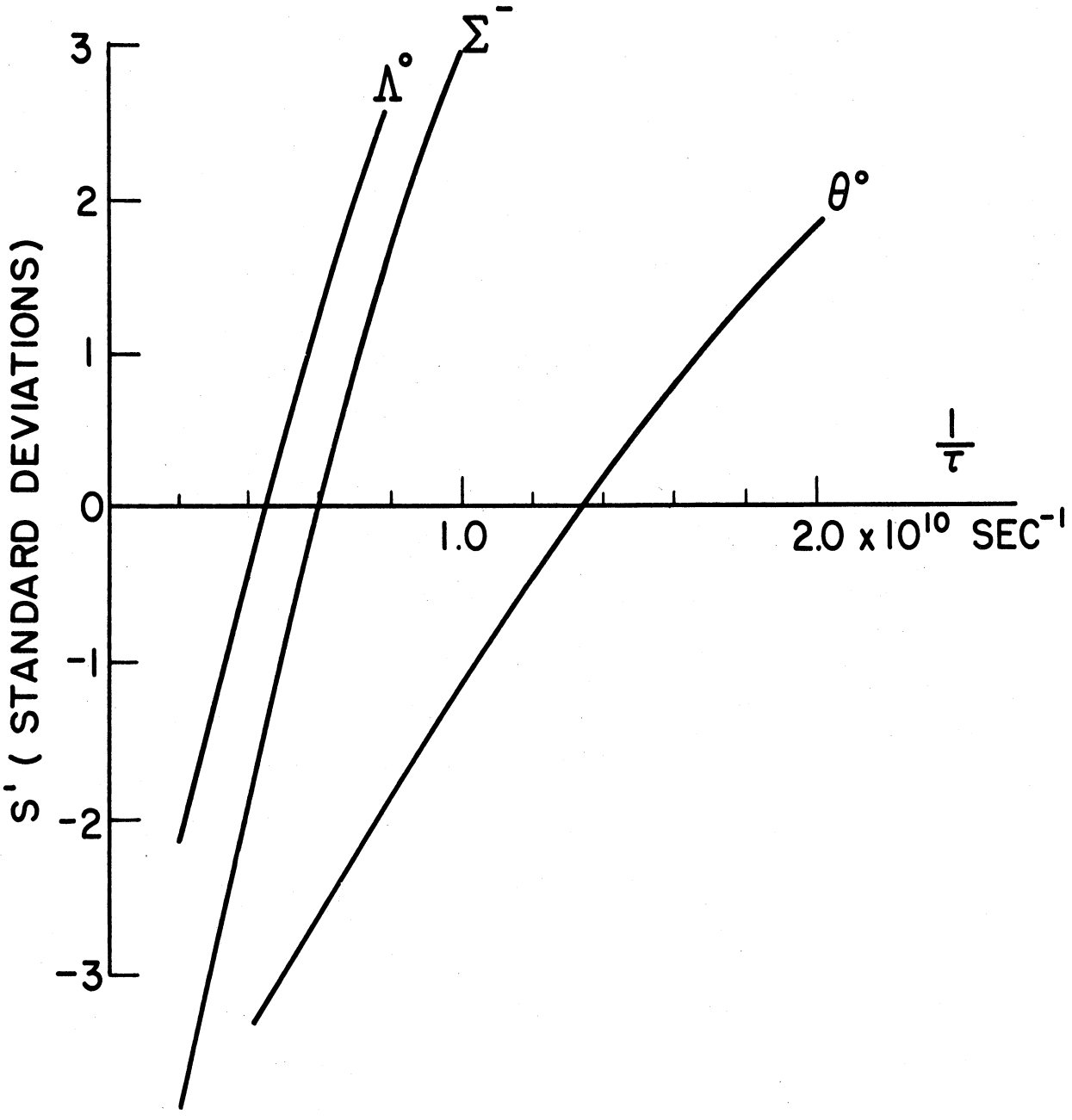

Figure 18. Lifetime Function for θ°, Λ°, Σ°.

in Reference 15. These angular distributions are defined in the rest system of the decaying strange particle. Referring to Fig. 19, we define the z axis as the line of flight of the strange particle, the y axis as the positive normal to the production plane (i.e., the direction of $\vec{P}_{\text{incident pion}} \times \vec{P}_{\text{hyperon}}$) and the x axis as the line perpendicular to the y and z axes (hence in the production plane). The π^- from the strange particle decay together with the z axis define a decay plane D. The azimuthal angle ϕ is the angle between the decay plane and production plane and can take on values between 0 and 2π. The latitude angle θ, which can take on values between 0 and π, is the center of mass decay angle of the baryon or π^+ with respect to the line of flight of the strange particle. For the θ° we can only determine $0 \leq \phi \leq \pi$, $0 \leq \theta \leq \pi/2$, since in general we cannot determine which of the decay products is the π^-. Also, for the Λ°'s produced in Σ° - θ° reactions the significance of the distribution $I(\phi)$ is not clear because of the intermediate decay of the Σ°.

The observed events have a distribution in θ averaged over ϕ, $I(\theta)$, and another distribution in ϕ averaged over θ, $I(\phi)$. The spin of the strange particle, the existence of parity doublets, and the conservation or non-conservation of parity in the strange particle decay will all affect the angular distribution $I(\theta)$ and $I(\phi)$. Unfortunately we can say little about the existence of parity doublets, since the effect of this phenomenon upon $I(\theta)$ and $I(\phi)$ requires a detailed knowledge of the production reaction which we do not possess.

If parity is not conserved in strange particle decay, there is no effect on the distribution $I(\theta)$, but the distribution $I(\phi)$ (for spin 1/2 particles) is of the form:

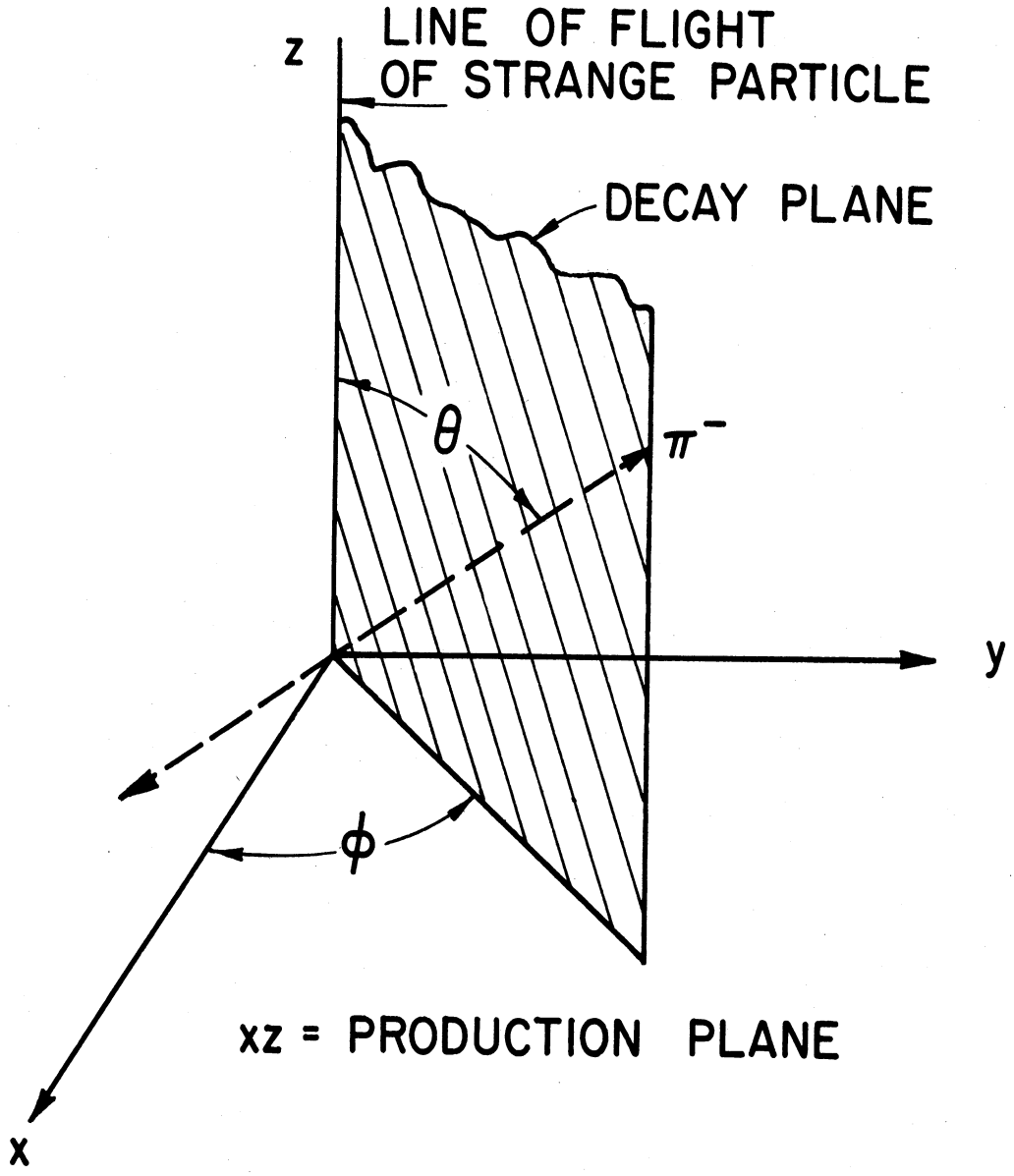

Figure 19. Coordinate System Used in Describing Strange Particle Decays

$$I(\phi) = (2/\pi)\ (1 + B_1 \sin \phi)$$

where $|B_1| \leq \pi/4$. The presence of the sin ϕ term arising from parity non-conservation means that:

$$I(\phi) \neq I(2\pi-\phi)$$

In view of the scarcity of the data, the only statistically significant test we can make to see if this term is present is to examine the ratio:

$$S = \frac{N\ (0 \leq \phi < \pi)}{N\ (\pi \leq \phi < 2\pi)} = \frac{1 + 2B_1/\pi}{1 - 2B_1/\pi} \leq 3$$

where $N(\phi_1 \leq \phi < \phi_2)$ is the number of events having ϕ in the indicated interval. For Λ°'s produced in Λ° - θ° reactions, we find $S(\Lambda^\circ) = 8/5$. If B_1 were actually zero, i.e., parity were conserved in Λ° decays, we would observe a value of S deviating this far or farther from unity 58% of the time. Two other events found in rescanning, which are not included in the above data, change the ratio to $S(\Lambda^\circ) = 8/7$, which is essentially unity. It should be noted, however, that very recent data from our laboratory and others (based on single V events) gives a strong indication that parity may actually <u>not</u> be conserved in the Λ° decay (16)(17)(18). For the Σ^- decays observed in this experiment, the value of the "up-down" ratio is S = 25/19. Again, if parity were conserved in the Σ^- decays, we would observe a value of S deviating this far or farther from unity 45% of the time. Data on Σ^- decays from other laboratories also does not indicate a value of S essentially different from unity. It is not clear at the time of writing why the Λ° should show evidence for parity non-conservation in its decay and the Σ^- should not. Finally, since for the θ° decays we cannot determine which of the decay products is the π^-, we cannot determine the ratio S.

We consider next the question of the intrinsic spins of the Λ°,

Σ^-, and θ°. For spin 0 or 1/2 particles $I(\phi)$ and $I(\cos\theta)$ are isotropic. Our experimental results are shown in Figs. 20 and 21, where we have folded our experimental distributions so that ϕ and θ run from 0 to $\pi/2$, in order to bring out any anisotropy.

For decaying Λ°'s arising from Λ° - θ° events, the data are too few to make a χ^2 test of the $I(\phi)$ distribution. (Remember that Λ°'s from Σ° - θ° events cannot be used in the $I(\phi)$ distribution because of the decay of the Σ°). The $I(\theta)$ distribution for Λ°'s from Λ° - θ° and Σ° - θ° events has a χ^2 probability of 0.1 of arising from an isotropic distribution. This should not be considered significant in view of a conceivable bias against decays with $\theta^\circ \sim 0^\circ$ due to the short π^- range. For the θ°, both the ϕ and θ distributions are consistent with spin 0, the χ^2 probabilities being 0.8 and 0.7, respectively. For the Σ^-, both the ϕ and θ distributions are consistent with spin 1/2, the χ^2 probabilities of these two distributions being 0.16 and 0.85, respectively. It should be mentioned that a different analysis has been made on the Σ^- data, utilizing the fact that those Σ^-'s produced in the forward direction are in a known state of polarization, so that their decay angular distributions uniquely determine their spin; calculations based on the combined data from several laboratories indicates that the Σ^- indeed has spin 1/2.

4.4 Possible Improvements

If this experiment were to be redone in order to determine more accurately results concerning cross sections, angular distributions, and lifetimes, several improvements immediately suggest themselves.

It is noted first that the largest source of error is almost invariably the small number of events. Either more pictures must be taken,

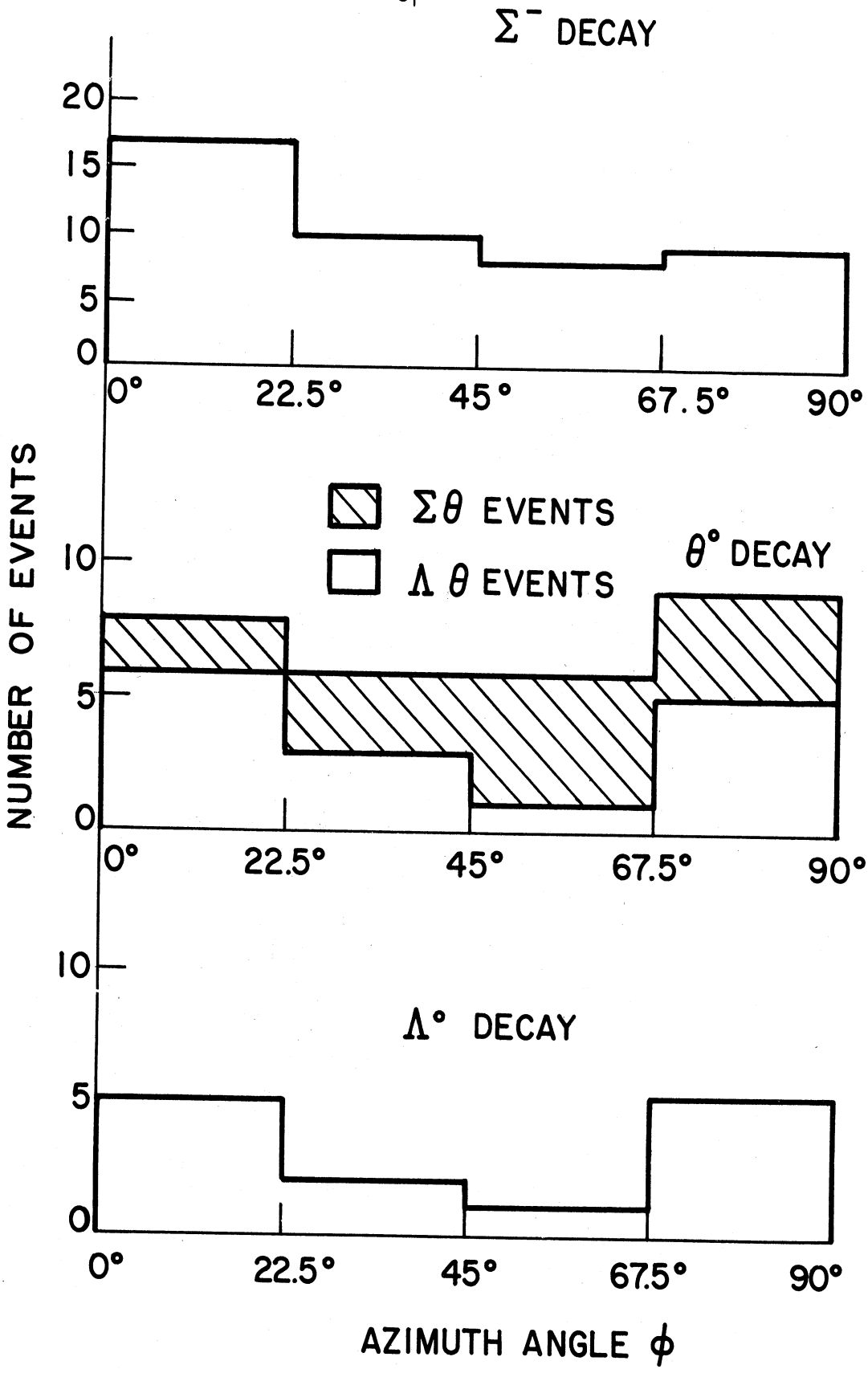

Figure 20. Angular Distribution I(∅) for Σ^-, θ°, and Λ° Decays

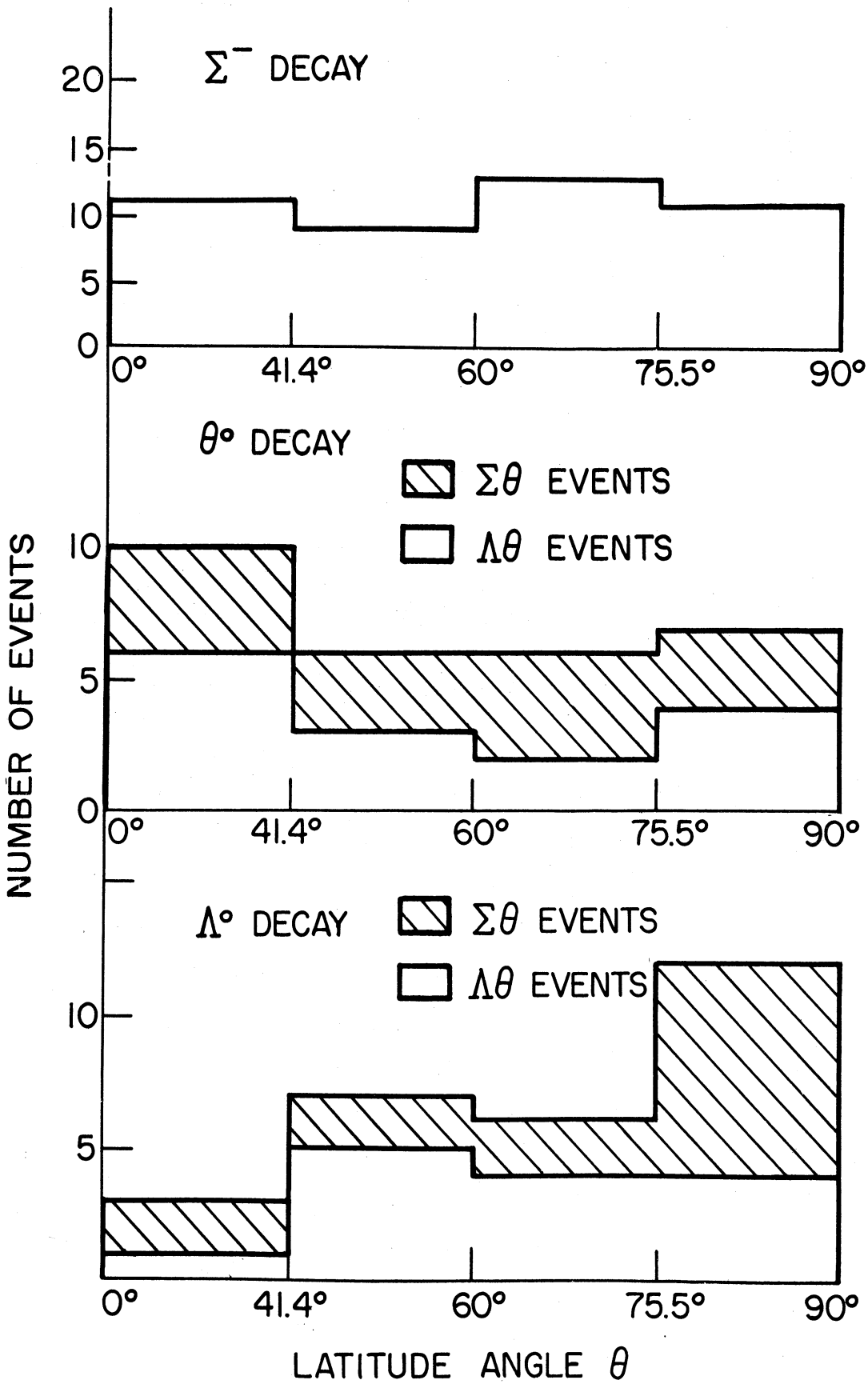

Figure 21. Angular Distribution I(θ) for Σ^-, θ°, and Λ° Decays

or a larger chamber used. It should be noted that the scanning effort will be roughly the same in either case, since it is essentially the number of miles of pion track that determines the scanning time.

Probably the second most important source of error comes from scanning. The scanning should be made easier and also more rigid. Better shielding and beam collimation would serve to remove most of the annoying background. Use of the cosmotron rapid beam ejector developed after this experiment was performed would serve to make all tracks the same size. Once cleaner pictures had been obtained, the scanning should be done according to rigid rules. This brings to mind mechanical scanning devices but no such practical device as yet exists. Certain mechanical aids could be used, however, to help scanners follow the various criteria. The final aim is not so much to make the scanning efficiency 100% as it is to make it a precise quantity.

Another source of error in this experiment was the carbon contamination, which was especially important in the case of $\Sigma^{\circ} - \theta^{\circ}$ events. The most obvious solution, of course, is the use of a hydrogen chamber. This is not an unmixed blessing, however; the technical difficulties in construction and operation are much greater than with a propane chamber, the hydrogen density is only half that of a propane chamber, and the stopping power only one-tenth. A simpler partial solution is the development of more accurate measuring techniques (equipment for which already exists) and of more elaborate computer programs to use more accurate camera formulas. A further aid would be better beam momentum analysis, which would narrow the acceptance criteria. With the aid of these improvements, the carbon contamination could be reduced by at least a factor of two. Parenthetically it might be added that a mag-

netic field would do little to help in this problem; its main use is as an aid to scanning, and also as an aid in utilizing carbon events.

4.5 Summary of Results

The associated production of strange particles 1.1 Bev kinetic energy π^- mesons by the reactions

$$\pi^- + p \rightarrow \Sigma^- + K^+$$

$$\pi^- + p \rightarrow \Lambda^\circ + \theta^\circ$$

$$\pi^- + p \rightarrow \Sigma^\circ + \theta^\circ$$

has been studied in a 12-inch propane bubble chamber. The total cross sections in hydrogen for the above reactions are 0.19 ± 0.05 mb, 0.24 ± 0.09 mb, and 0.17 ± 0.07 mb, respectively. In the π^- - p center of mass, the Σ^- is produced in the forward direction while the Λ° and Σ° are produced in the backward direction. Lifetimes for the Σ^-, Λ°, and θ° are found to be $1.67\ {}^{+0.48}_{-0.28} \times 10^{-10}$ seconds, $2.24\ {}^{+0.79}_{-0.48} \times 10^{-10}$ seconds, and $0.74\ {}^{+0.21}_{-0.15} \times 10^{-10}$ seconds, respectively. From various angular distributions of decay products we find that the data are consistent with spin 1/2 for the Λ° and the Σ^- and spin 0 for the θ° The data are also consistent with parity conservation in strange particle decay.

BIBLIOGRAPHY

1. Rochester and Butler, Nature, 160, 855, (1947).
2. Shapiro, Rev. Mod. Phys. 28, 164 (1956).
3. Plano, Samios, Schwartz and Steinberger, Nevis Report No. 38.
4. Lande, Lederman, and Chinowsky, Nevis Report No. 29.
5. Progress in Cosmic Ray Physics, Vol. III, p. 155, 1956.
6. Fowler, Shutt, Thorndike, and Whittemore, Phys. Rev. 91, 1287 (1953).
7. Walker, Phys. Rev. 98, 1407 (1955) and Walker and Shephard, Phys. Rev. 101, 1810 (1956).
8. D. C. Rahm, thesis, The University of Michigan, 1956 (unpublished).
9. Glaser, Rahm, and Dodd, Phys. Rev. 102, 1653 (1956).
10. Willis, Fowler, and Rahm, Phys. Rev., to be published.
11. J. C. VanderVelde, private communication.
12. G. Puppi, private communication to D. A. Glaser.
13. Plano, Samios, Schwartz, and Steinberger, Nevis Report No. 46.
14. M. S. Bartlett, Phil. Mag. 44, 249 (1953).
15. Morpurgo, Nuovo Cimento 3, 1069 (1956); 4, 1222 (1956).
16. C. Graves, private communication.
17. F. Crawford, et al., UCRL Report No. 8008.
18. J. Steinberger, private communication.

APPENDIX A. DERIVATION OF KINEMATICAL RELATIONSHIPS

In this appendix we shall indicate the manner in which the kinematical relationships displayed in Figs. 4, 6, 8, 10, 11, 12, and 13 are obtained. The following assumptions are made:

1) energy and momentum are conserved in any production or decay; and
2) the quantity $(\vec{p}, iE/c)$ transforms like a four-vector under Lorentz transformations, where $\vec{p}$ is the three-vector momentum E is the total energy, and c is the velocity of light.

Let us consider a reaction of the type:

particle "I" + particle "II" → particle 1 + particle 2

This can be represented schematically in the laboratory and center of mass systems as follows:

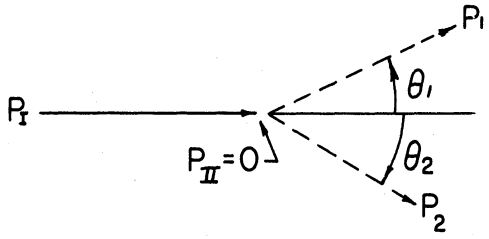

$\vec{P} = \vec{P}_I + \vec{P}_{II} = \vec{P}_1 + \vec{P}_2$

laboratory system

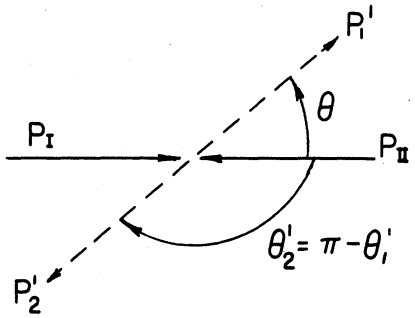

$\vec{P}' = \vec{P}_I' + \vec{P}_{II}' = \vec{P}_1' + \vec{P}_2'$

center of mass system

where p_i represents the momentum of the i^{th} particle. Primed quantities refer to the center of mass system. Let us immediately specialize to the case where $p_{II} = 0$. This corresponds, for example, in the reaction $\pi^- + p \rightarrow \Lambda^\circ + \theta^\circ$, to considering only those cases in which the proton is at rest (i.e. in hydrogen).

The center of mass system is defined as that coordinate system in which the total momentum of the particles, $\vec{p}'$, is zero. The center of mass system will thus be moving with respect to the laboratory system with a velocity β (in units of c), whose direction is that of $\vec{p}$, the total momentum in the laboratory system. Writing down the Lorentz transformation for momentum (when β is in the direction of $\vec{p}$), we have:

$$p' = \frac{p - \frac{\beta E}{c}}{\sqrt{1 - \beta^2}}$$

where E is the total energy in the laboratory system. Since we have defined the center of mass system as that one in which $\vec{p}' = 0$, we have:

$$\beta = \frac{pc}{E} \qquad (1)$$

as the velocity of the center of mass system with respect to the laboratory system, in terms of p and E.

Then for the energy and momentum before the collision in the laboratory system, we can write:

$$E = \sqrt{m_I^2 c^4 + p_I^2 c^2} + \sqrt{m_{II}^2 c^4 + p_{II}^2 c^2} \qquad (2a)$$

$$\vec{p} = \vec{p}_I + \vec{p}_{II} \qquad (2b)$$

where m_i represents the rest mass of the i^{th} particle.

The magnitude of the four-vector $(\vec{p}, iE/c)$ is an invariant, i.e. the quantity:

$$N = \sqrt{E^2 - p^2c^2} = \sqrt{E'^2 - p'^2c^2} \qquad (3)$$

is an invariant. We choose to evaluate this in the center of mass system. The total momentum of the particles in the center of mass system is zero, hence by the conservation of momentum $\vec{p}_1' = -\vec{p}_2'$. If we let $|\vec{p}_1'| = |\vec{p}_2'| = b$, we then have:

$$N^2 = (m^2c^4 + b^2c^2) + (m^2c^4 + b^2c^2) + 2\sqrt{(m^2c^4 + b^2c^2)(m^2c^4 + b^2c^2)}$$

This can be solved for the center of mass momentum, b, of the outgoing particles 1 or 2, to give:

$$b = \frac{1}{2Nc}\sqrt{[N^2-(m_1 - m_2)^2c^4]\,[N^2-(m_1 + m_2)^2c^4]} \qquad (4)$$

We now want to transform this center of mass momentum into the laboratory system; if we call the x axis the direction of $\vec{\beta}$, we have:

$$p_{1x} = \frac{p'_{1x} + \frac{\beta E_1'}{c}}{\sqrt{1 - \beta^2}} \qquad (5a)$$

$$p_{1y} = p'_{1y} \qquad (5b)$$

$$p_{1z} = p'_{1z} \qquad (5c)$$

as the Lorentz-transformed momentum for particle 1 (similarly for particle 2). In eqn. (5a), E_1' is the total energy of particle 1 evaluated in the center of mass system:

$$E_1' = \sqrt{m_1^2c^4 + b^2c^2} \qquad (6)$$

and similarly for E_2'.

Now, referring back to our vector diagrams, we have in the laboratory system:

$$\cos \theta_1 = \frac{p_{1x}}{p_1} = \frac{p_{1x}}{(p_{1x}^2 + p_{1y}^2 + p_{1z}^2)^{1/2}} \qquad (7a)$$

$$\cos \theta_2 = \frac{p_{2x}}{p_2} = \frac{p_{2x}}{(p_{2x}^2 + p_{2y}^2 + p_{2z}^2)^{1/2}} \qquad (7b)$$

while in the center of mass system, we have:

$$p'_{1x} = p'_1 \cos \theta'_1 = b \cos \theta'_1 \qquad (8a)$$

$$p'_{2x} = p'_2 \cos \theta'_2 = b \cos (\pi - \theta'_1) \qquad (8b)$$

Assuming in all cases that all the masses are known constants, let us choose some value of p_I, i.e., some value of the incident beam momentum. We can then find E and $\vec{p}$ by eqn. (2), and then β by eqn. (1). We can also find N by (3) and hence b by (4), and E'_1 (and E'_2) by (6). Then choosing some value of θ'_1 (center of mass production angle) we can calculate θ_1 and θ_2 as functions of p_I and θ'_1, using (8), (5), and (7). In this fashion the curves displayed in Figs. 4, 6, and 8 were calculated.

If, instead of θ_1 vs. θ_2, we wish to plot p_1 vs. θ_1, we calculate θ_1 as before, and find p_1 from, say, eqn. (7). The curves in Figs. 12 and 13 were calculated in this way.

To calculate the kinematics relevant to the decay of a particle, one can use all of the equations just derived, setting $m_{II} = 0$, and identifying particle I as the decaying strange particle, and particles 1 and 2 as its decay products. Then one can calculate θ_1 and θ_2 as functions of p_I (the strange particle momentum in the laboratory system) and θ'_1 (the center of mass decay angle). Thus the curves of Figs. 10 and 11 were generated.

APPENDIX B

TABLES OF DATA FOR INDIVIDUAL EVENTS

Table 9. Data for $\pi^- + p \rightarrow \Lambda^\circ + \theta^\circ$ Events in Hydrogen

Frame Number	α	θ_Λ	φ_Λ	θ_θ	φ_θ
14609	115°	120°	285°	87°	79°
15707	137°	119°	3°	88°	90°
17440	103°	62°	147°	28°	12°
17864	167°	120°	195°	89°	163°
24051	137°	106°	202°	27°	19°
29497	175°	67°	76°	61°	140°
29992	138°	143°	126°	37°	31°
31557	109°	129°	37°	18°	98°
32181	160°	56°	345°	52°	73°
32238	167°	97°	not measurable	52°	75°
35859	174°	46°	5°	10°	175°
36023	133°	--	anomalous Λ° --	60°	50°
36081	140°	79°	92°	79°	152°
36542	147°	121°	286°	59°	97°
38846	87°	45°	91°	36°	176°

α is the Λ° production angle in the π^- - p center of mass system

θ_Λ is the π^- decay angle in the Λ° center of mass system.

φ_Λ is the angle between the decay plane of the Λ° and production plane as defined in Fig. 19.

θ_θ is the θ° center of mass decay angle; $0^\circ \leq \theta_\theta \leq 90^\circ$ since we cannot generally distinguish between the π^+ and π^-.

φ_θ is the angle between the decay plane of the θ° and the production plane; $0^\circ \leq \varphi \leq 180^\circ$ since we cannot distinguish π^+ and π^-.

Table 10. Data for $\pi^- + p \rightarrow \Sigma^\circ + \theta^\circ$ Events in Hydrogen

Frame Number	α	θ_Λ	φ_Λ	θ_θ	φ_θ
16185	130°	93°		86°	149°
17365	92°	83°		20°	170°
18011	167°	85°		61°	81°
19485	62°	62°		38°	82°
19686	138°	65°		31°	15°
25759	127°	77°		65°	58°
27868	128°	132°		53°	74°
28260	148°	92°		85°	117°
28415	105°	101°		61°	71°
33769	97°	99°		86°	101°
34659	155°	77°		74°	165°
35785	147°	136°		51°	117°
36099	50°	151°		18°	9°
36266B	27°	165°		44°	124°

α is the Σ° production angle in the π^- - p center of mass system.

φ_Λ is not included because of the intervening Σ° decay; all other angles are the same as in Table 9.

Table 11. Data for $\pi^- + p \rightarrow \Sigma^- + K^+$ Events in Hydrogen

Frame Number	α	θ_Σ	ϕ_Σ
7968	77°	70°	97°
9510	60°	100°	257°
9942	97°	117°	20°
11882	24° (K_s)	53°	34°
12472	95° (K_f)	--	--
12920	52°	97°	87°
13633	107°	50°	294°
13638	87°	142°	330°
13893	81° (K_f)	98°	118°
14020	29° (K_s)	152°	301°
14356	36°	105°	346°
15084	66°	119°	39°
15115	36° (K_s)	141°	352°
17080	61°	97°	248°
17441	88°	145°	162°
18319	112°	69°	139°
19019	73°	95°	211°
19427	96°	170°	130°
20165	59°	96°	10°
20756	40° (K_s)	--	--
20849	15° (K_s)	--	--
21103	52°	91°	170°

Table 11. Data for $\pi^- + p \rightarrow \Sigma^- + K^+$ Events in Hydrogen (con't)

Frame Number	α	θ_Σ	φ_Σ
21134	88°	113°	265°
22000	46°	--	--
22160	72°	78°	175°
22246	72°	68°	7°
25035	125°	15°	179°
25765	78°	145°	28°
26496	87°	146°	16°
26733	89°	143°	351°
26773	82°	68°	302°
26986	104°	135°	76°
27012	57° (K_f)	75°	13°
27683	113°	100°	136°
28093	48°	108°	277°
30072	61°	78°	101°
30083	30° (K_s)	48°	345°
30727	88°	23°	326°
32475	94°	72°	328°
32839	32° (K_s)	58°	34°
32898	48°	137°	80°
32991	42° (K_s)	--	--
35834	34° (K_s)	--	--
35877	40°	99°	20°
35879	34° (K_s)	--	--

Table 11. Data for $\pi^- + p \rightarrow \Sigma^- + K^+$ Events in Hydrogen (con't).

Frame Number	α	θ_Σ	φ_Σ
36137	91°	21°	32°
36289	78°	124°	48°
36333	10°	74°	310°
37469	37°	132°	314°
37703	112°	58°	348°
37799	54°	107°	187°

α is the Σ^- production angle in the π^- - p center of mass system.

θ_Σ is the π^- decay angle in the Σ^- center of mass system.

φ_Σ is the angle between the decay plane of the Σ^- and the production plane as defined in Fig. 19.

K_s and K_f noted after the center of mass production angle refer to events in which the K^+ stopped or decayed in flight, respectively.

A blank in the θ_Σ and φ_Σ columns refers to those events in which the Σ^- decay was either not observed or not measurable.